学位論文(要約)

Stability control of antisense long non-coding RNA and its role in gene regulation

(アンチセンス長鎖非コードRNAの安定性制御と遺伝子発現における役割)

平成 28 年 12 月博士 (理学) 申請

東京大学大学院理学系研究科

生物科学専攻

三木 敦子

TABLE OF CONTENTS

Abstract

Antisense RNA can be categorized into a type of long non-coding RNAs (lncRNAs), which have been recognized as important transcriptional regulators for protein-coding genes. However, little is known about their dynamics and decay process, especially in a context of stress response. Antisense RNAs transcribed from the fission yeast *fbp1* locus (*fbp1-as*) are expressed in glucose-rich condition. Importantly, during glucose starvation, they show anti-correlated pattern with the sense-strand transcription of metabolic stress-induced lncRNA (mlonRNA) and mRNA. Although the characters and decay mechanisms of sense mlonRNAs and mRNA have been demonstrated extensively, those of antisense RNAs have not yet been uncovered.

In this study, I investigated the localization and decay of *fbp1-as* and antisense RNAs from other glucose-stress responsive loci, and propose a model to explain the rapid switch between antisense and sense mlonRNA/mRNA transcription triggered by glucose starvation. I first demonstrated that *fbp1-as* was 5'-capped and poly(A)-tailed like mRNAs. Decay of *fbp1-as* at least partly required Rrp6, a component of the nuclear exosome complex for 3' to 5' RNA degradation. Polysome fractionation and single molecule fluorescence *in situ* hybridization (smFISH) revealed that *fbp1-as* molecules were mostly detected in the cytoplasm. Interestingly, they were bound to poly-ribosomes in glucose-rich conditions. Furthermore*, fbp1-as* as well as antisense RNAs at other glucose

stress-responsive loci were rapidly degraded *via* the co-translational nonsense-mediated decay (NMD) pathway. These results suggest that NMD may accelerate in response to cellular stress the swift turnover from antisense RNAs to sense ones in some stress-related loci.

Abbreviations

3’RACE	3’-rapid amplification of cDNA ends
5’cap	5’ 7-methylguanosine (m_7G) cap structure
BSA	bovine serum albumin
cAMP	cycric adenosine monophosphate
cap-IP	immunoprecipitation using an anti-5’-cap antibody
ChIP	chromatin immunoprecipitation
CHX	cycloheximide
CLRC complex	Clr4-Rik1-Cul4 complex
CTP	cytidine triphosphate
CUTs	Cryptic unstable transcripts
DAPI	4', 6-diamidino-2-phenylindole
dCTP	deoxycytidine triphosphate
DNA	deoxyribonucleic acid
EDTA	ethylenediaminetetraacetic acid
fbp1-as	antisense transcripts from *fbp1* locus
HEPES	4-(2-hydroxyethyl)-1-piperazineethanesulfonic acid
lncRNA	long non-coding RNA
MAPK	mitogen-activated protein kinase
MAPKK	mitogen-activated protein kinase kinase
MAPKKK	mitogen-activated protein kinase kinase kinase

miRNA	microRNA
mlonRNA	metabolic stress-induced long non-coding RNA
mRNA	messenger RNA
NMD	nonsense-mediated decay
NNS complex	Nrd1-Nab3-Sen1 complex
nt	nucleotide
NUTs	Nrd1-unterminated transcripts
ORF	open reading frame
PCR	polymerase chain reaction
per1-as	*Per1* antisense RNA (*SPNCRNA.934.1*)
piRNA	Piwi-interacting RNA
PKA	protein kinase A
poly(A)-tail	3’ polyadenylation tail
PRC2	polycomb repressive complex2
PROMPT	promoter-associated pervasive transcript
qPCR	quantitative PCR
RACE	rapid amplification of cDNA ends
ribo-seq	ribosome profiling
RITS	RNA-induced initiation of transcriptional gene silencing
RNA	ribonucleic acid
RNAi	RNA interference

RNA pol II	RNA polymerase II
rRNA	ribosomal RNA
RT	reverse transcription
SDS	sodium dodecyl sulfate
siRNA	small interference RNA
smFISH	single-molecule fluorescence *in situ* hybridization
sORF	small open reading frame
SSC	saline sodium citrate
STRE	stress response element
SUTs	Stable unannotated transcripts
TINCR	terminal differentiation-induced ncRNA
TRAMP	Trf4/Air2/Mtr4 polyadenylation
TRAP	translating ribosome affinity purification technique
tRNA	transfer RNA
TSS	transcription start site
UAS	upstream activating sequence
UPAT	UHRF1 (ubiquitin-like PHD and RING finger domain-containing protein 1)-associated transcript
UTR	untranslated region
XIST	X-inactive specific transcript
XUTs	Xrn1-sensitive unstable transcripts

Introduction

1. Discovery of non-coding RNA

There has been an ongoing debate that the numbers of protein-coding genes cannot explain the complexity of higher organisms. For example, only 1.5 % of the human genome encodes protein (reviewed in Taft *et al*. 2007). The haploid genomic DNA content (referred to as C-value) is not proportional to the complexity of each organism; hence the above-mentioned paradox has been called 'the C-value paradox' (reviewed in Gall, 1981; see also http://www.genomesize.com/).

The recent highly improved next generation sequencing technology, however, has uncovered numerous unannotated transcripts without protein coding potential in various species. For instance, about 70-90% of the human genome is transcribed at least on some occasion during differentiation and in developed bodies (reviewed in Kung *et al*. 2013). Since the variety of such non-coding transcripts is higher as the complexity of the organism increases, complexity of non-coding DNA segments of higher organisms may solve the C-value paradox.

2. Long non-coding RNAs and their function

Unannotated non-coding transcripts had long been thought as transcriptional noise or junk. However, the discovery of transfer RNAs (tRNAs, Holley *et al*. 1965) in 1960s and discovery of ribosomal RNAs (rRNAs) in 1970s (reviewed in

Brimacombe & Stiege, 1985) led us to realize that some non-coding RNAs are functional.

Up to now, several categories of non-coding RNAs have been identified. Long noncoding RNAs (lncRNAs), arbitrarily defined as RNAs longer than 200 nucleotides, seemingly have different functions from those of tRNAs, small interference RNAs (siRNAs), Piwi-interacting RNAs (piRNAs), and microRNAs (miRNAs).

Some of the lncRNAs have been demonstrated to play roles in gene regulation at stages of transcription, RNA decay/quality control, translation, and degradation of proteins. During transcription, lncRNAs play regulatory roles by interacting with other proteins (e.g. transcription factors, chromatin remodelers, and histone modifiers) to recruit them to their target genes (Rinn *et al.* 2007). Translation of specific target mRNAs is also affected by lncRNAs. For example, lncRNA-p21 can inhibit the translation of target mRNA (Yoon *et al.* 2012). Some RNAs and proteins are specifically stabilized by lncRNAs such as TINCR (terminal differentiation-induced ncRNA) and UPAT (UHRF1 (ubiquitin-like PHD and RING finger domain-containing protein 1)-associated transcript) (Kretz *et al.* 2013; Taniue *et al.* 2016).

3. Antisense RNA

Antisense RNAs, which are transcribed from the opposite strand of the sense protein-coding RNA, are also classified as non-coding RNA. Antisense transcripts are observed in a wide range of taxa including mammals, plants, insects, bacteria, archeae, and fungi (Zhang *et al.* 2006), though the frequency of annotated loci expressing overlapping antisense RNAs is variable among organisms. It should be noted that some, if not all, antisense RNAs are suggested to function in gene regulation.

The antisense-mediated gene regulation was first discovered in bacterial plasmids and bacteriophages (Tomizawa *et al.* 1981; Krinke & Wulff 1987). As early as 1990s, it was revealed that XIST (X-inactive specific transcript), a lncRNA important for X chromosome inactivation, was antagonistically regulated by the antisense transcript Tsix (Lee *et al*. 1999). Subsequently, many antisense lncRNAs began to be reported as regulators of the expression of overlapping sense RNA in various organisms, and through several mechanisms. For example, LUC7L silences its corresponding sense RNA expression through DNA methylation in human (Tufarelli *et al*. 2003), RME2 through transcriptional interference (Hongay *et al*. 2006), WDR83 through RNA stability (Su *et al.* 2012), respectively. For chromatin modification-mediated sense RNA regulation, Coolair (*Arabidopsis*, Swiezewski *et al*. 2009), PHO84 (*S.cervisiae,* Camblong *et al.* 2007*)*, ANRIL (Human, Yap *et al*. 2010), and others are reported. Uchl1,

carrying short interspersed elements (SINEs), enhances the translation of mRNAs by their complementary sequences (Carrieri *et al.* 2012).

Another type of antisense RNA-mediated mechanism is direct base complementarity to regulate translation level (Yoon *et al.* 2012). Furthermore, genome-wide studies in yeast suggest that many antisense RNAs are associated with stress-responsive loci (Ni *et al.* 2010; Bitton *et al.* 2011; Leong *et al.* 2014). However, the precise mechanism underlying quick sense/antisense RNA transcript switching during stress response is still unknown.

4. Fission yeast *Schizosaccharomyces pombe* (*S. pombe*) and stress response

The fission yeast *Schizosaccharomyces pombe* (*S. pombe*) is a good model eukaryotic organism, in which a lot of genetic tools are available. Importantly, basic signal molecular mechanisms in human cells are also conserved in *S. pombe*. Therefore, molecular mechanisms of gene regulation, cell cycles, and stress response have been intensively investigated in *S. pombe*. In this study, I focus on glucose starvation, under which yeast cells are running short of glucose, the most important energy and carbon sources for many organisms. Under glucose rich condition, cells utilize glucose as a major energy source through the glycolysis pathway. On the other hand, when cells encounter glucose starvation, the gene expression pattern in the cell changes drastically. In the

glucose-starved condition, the gluconeogenesis pathway is activated to synthesize glucose from other non-carbohydrate carbon sources such as glucogenic amino acids and lipids. The gluconeogenesis pathway requires induction of an enzyme called fructose-1,6-bisphosphatase 1 (Fbp1), the expression of which is strictly repressed under glucose rich conditions (Fig. 1).

Transcription of *fbp1* mRNA is regulated by transcription factors, Atf1-Pcr1 and Rst2 (Fig. 2). Upon glucose starvation, the stress-activated mitogen-activated protein kinase (MAPK) pathway is activated. This MAPK pathway involves a MAP kinase cascade of Wis4 or Win1 (MAPKKK), Wis1 (MAPKK), and Spc1/Sty1 (MAPK) (Takeda *et al.* 1995; Millar *et al.* 1995; Shiozaki and Russell 1995,1996; Warbrick and Fantes 1991; Samejima *et al*. 1997,1998). Activated Sty1 then phosphorylates a CREB/ATF-type transcription factor Atf1 which forms a heterodimer with Pcr1 (Watanabe and Yamamoto, 1996). The Atf1-Pcr1 heterodimer binds to a *cis*-acting DNA sequence called the cAMP response element (CRE) (Hai *et al*. 1988; Roesler *et al*. 1988). The upstream region of *fbp1* locus has a CRE-like element called UAS1 (upstream activating sequence 1), to which the binding of the Atf1-Pcr1 complex is enhanced in response to glucose starvation (Neely and Hoffman, 2000). Another important signaling pathway is the PKA/cAMP (cycric AMP) pathway. Under glucose rich condition, high glucose concentration is sensed by a G protein-coupled receptor (Git3) and associated G proteins (Gpa2, Git5, and Git11) (Welton and Hoffman, 2000). Gpa2 is activated when high extracellular

glucose is detected, leading to an activation of adenylate cyclace (AC, Cyr1) which up-regulates PKA kinase activity. Upon glucose starvation, the activity level of PKA in the cell is down-regulated, which leads to activation of a C_2H_2 Zn-finger transcription factor Rst2. There is a STRE (stress response element)-like element in the upstream of *fbp1* locus (UAS2, upstream activating sequence 2), and Rst2 binds to this site upon glucose starvation (Higuchi *et al*. 2002). In summary, *fbp1* expression is under the stringent control of a pair of complementary signal transduction pathways and transcription factors.

5. Long non-coding RNAs transcribed during glucose starvation in *S. pombe*

The *S. pombe* genome has long intergenic regions without apparent protein-coding genes. However, non-coding transcripts are often expressed from these regions. The 5' upstream segment of *fbp1* gene also produces non-coding transcripts. Before the full induction of *fbp1* mRNA, a cascade of long non-coding RNA transcription occurs from the 5' upstream of *fbp1* coding sequence (Fig. 3, left, cited from Oda *et al.* 2015). Such non-coding transcripts are referred to as mlonRNA (metabolic stress-induced lncRNA) (Hirota *et al.* 2008). In glucose-rich conditions, chromatin accessibility is reduced by the action of Groucho/Tup-family global transcriptional corepressors Tup11 and Tup12 (Hirota *et al.* 2003). However, upon glucose starvation, transcription of

mlonRNA locally promotes chromatin remodeling at least partly by antagonizing Tup11 and Tup12 repressors (Takemata *et al.* 2016). Interestingly, under glucose rich condition, antisense lncRNA is expressed from the entire region covering both *fbp1* locus and its upstream region (Rhind *et al.* 2011). This antisense RNA quickly fades out upon glucose starvation (Fig. 3A, right, cited from Oda *et al.* 2015). Though the regulation mechanisms of sense RNAs (mlonRNA and mRNA) are intensively investigated, the characteristics and the regulatory mechanisms of antisense RNA expression remain unclear.

6. RNA quality control system in the cells

Steady-state levels of RNA are determined by the balance between transcription and degradation, and therefore, RNA degradation is one of the important steps to regulate RNA expression.

The endpoint of RNA degradation has been shown to be RNA decay from either 5'-ends or 3'-ends by highly conserved directional exonucleases. In fission yeasts, 5'-exonucleases Exo2 (Xrn1 in *S.cervisiae*) and Dhp1 (Rat1 in *S.cervisiae*) localize in the cytoplasm and nucleus (reviewed in Houseley *et al.* 2006), respectively. On the other hand, degradation from the 3'-end is catalyzed by the exosome complex, composed of a ring of 9 essential subunits including Dis3, associated with compartment-specific cofactors, either Rrp6 in the nucleus or Ski2 in the cytoplasm (reviewed in Parker 2012, Fig. 4).

In general, RNA transcripts are classified according to which exonuclease is thought to degrade them. Budding yeast CUTs (Cryptic Unstable Transcripts) and human PROMPTS (promoter-associated pervasive transcripts) are detectable only when the nuclear exosome is deficient (Wyers *et al.* 2005; Preker *et al*. 2008). In budding yeast, NUTs (Nrd1-Unterminated Transcripts) are visible upon depletion of Nrd1, a nuclear RNA-binding factor (Schulz *et al.* 2013), and XUTs (Xrn1-sensitive unstable transcripts) are also observed in mutants of the cytosolic exonuclease *XRN1* (van Dijk *et al.* 2011). On the other hand, SUTs (Stable Unannotated Transcripts) can be detected even in wild type cells (Xu *et al.* 2009). Rrp6 targets many kinds of RNAs through interaction with Nrd1–Nab3–Sen1 (NNS) complex (Vasiljeva & Buratowski 2006). NNS complex has binding motif and involved in termination of RNAs, thus enables cells to degrade both CUTs and NUTs which possess improperly processed 3' ends (Fox *et al*. 2015).

However, it should be pointed out that many of these studies only focused on steady-state level and did not directly estimate the half-lives of transcripts. Therefore, it is plausible that the reported results can be partly due to secondary effects of the absence of those nucleases. Recently, Wery *et al.* demonstrated that antisense-sense RNA pairs may protect each other from ribosome accessibility and that NMD degradation was triggered depending on the extent of their overlap. This interesting mechanism remains to be investigated in the context of a stress response.

Despite the lack of apparent protein-coding potential, some non-coding RNAs can evade from nuclear RNA decay systems, and are exported to the cytoplasm. They then heavily associate with ribosomes (Galipon *et al.* 2013; Guttman *et al.* 2013), which ultimately cause translation-coupled RNA degradation by RNA quality control pathways such as nonsense-mediated decay (NMD) (Smith *et al.* 2014; Wery *et al.* 2016). In NMD, premature translation termination occurring at aberrant stop codons triggers the assembly of the Upf1/2/3 complex, followed by endonucleolytic RNA cleavage, decapping or deadenylation (reviewed in Schoenberg & Maquat 2012). However, the role of canonical RNA degradation pathways such as NMD in the regulation of stress-responsive lncRNA remains elusive.

7. Protein coding ability of RNAs

Which parts of RNAs are targeted to ribosomes and to what extent the RNAs are translated into proteins have long been important questions to be answered. Two types of new technologies to investigate ribosomal association on RNAs and their translating landscape recently became available. The first one is “TRAP (translating ribosome affinity purification technique)/Ribo-tag”. In this method, epitope-tagged ribosomes are purified and their associating mRNAs are isolated for deep-sequencing (Heiman *et al.* 2008). The other is “ribosome profiling” (ribo-seq, Ingolia *et al*. 2009). This technology, cycloheximide (CHX) or

another translation inhibitor is added to the cell lysate to halt the progression of ribosomes, and RNase I is then added to degrade the RNA regions that are not associated with ribosomes. RNA fragments bound to ribosomes are protected from RNase I-dependent, and can therefore be extracted, tagged, and reverse transcribed to generate libraries for next generation sequencing (NGS) analysis (Fig. 5). The latter method enables to determine the exact ribosome binding sites genome-widely at nucleotide resolution.

Although ribo-seq studies have confirmed the presence of ribosomes on lncRNAs, whether they are translated into proteins or short peptides is still unclear. Computational analysis revealed that most of them are not translated into proteins (Guttman *et al.* 2013), though it is noted that there are several non-coding RNAs associated with ribosomes to produce small peptides (Kondo *et al*. 2010; Aspden *et al*. 2014; Nelson *et al*. 2016). However, the fate and decay processes of such ribosome-bound lncRNA are largely unknown.

8. Transcription and histone modification

Another important aspect of lncRNAs is their role in controlling epigenetic modifications. For example, in *S. pombe*, heterochromatic regions are silenced by siRNA-based mechanisms. The RITS complex (RNA-induced initiation of transcriptional gene silencing complex) is recruited by small RNAs originating from centromeric repeat regions (Verdel *et al.* 2004), and in turn locally recruits

Chp1 and the Clr4-Rik1-Cul4 (CLRC) methyltransferase/ubiquitin ligase complex, which is important for assembly and maintenance of heterochromatin (Zhang *et al*. 2008). Another famous example of RNA-mediated chromatin modification is *XIST* in placental mammals, which recruits the polycomb repressive complex 2 (PRC2) to the X chromosome, thus enables X chromosome inactivation. Furthermore, the yeast PHO84 region is a well-characterized region where the transcription of short antisense RNA transcripts (CUTs) is terminated by the NNS complex, which in turn recruits the Set1 methyltransferase complex (Ng *et al*. 2003), thus repressing transcription of sense RNA from the 5' promoter region (Castelnuovo *et al*. 2013).

9. Aim and summary of this study

Though antisense RNAs are prevailing among stress-responsive loci, their characteristics and regulation mechanisms remain elusive. In *S. pombe* glucose bidirectional stress-responsive *fbp1* region, the induction and decay mechanisms of *fbp1* sense non-coding RNAs (mlonRNA) and *fbp1* mRNA were thoroughly investigated, however, very little is known about their overlapping antisense counterpart.

In this study, I extensively characterized the antisense RNA transcribed from the *fbp1* locus (*fbp1-as*) in *S. pombe*, especially its localization, decay (RNA half-life and degradation pathways), ribosomal association, and dynamics in

response to glucose starvation. In addition, the generality of decay dynamics of antisense RNAs from stress-responsive loci was tested genome-wide using RNA-seq and Ribo-seq data. I also investigate the mechanism of transcriptional switching in *fbp1* locus from antisense to sense directions particularly from the point of view of histone modifications.

It was revealed that *fbp1-as* is polyadenylated and 5'-capped. Most of *fbp1-as* were degraded by the nuclear exosome, but some of them were exported to the cytoplasm and bound to ribosomes. The ribosomal association of *fbp1-as* led to constitutive rapid decay by the NMD machinery in the cytoplasm. In addition, similar decay dynamics were observed for antisense RNAs from other glucose stress-responsive loci. It is likely that the constitutive rapid decay of those antisense RNAs accelerate the turnover from antisense RNAs to sense ones at some bidirectional loci in response to stress. These results suggest that NMD-dependent decay facilitate the transcriptional inversion from antisense to sense transcription in response to glucose starvation.

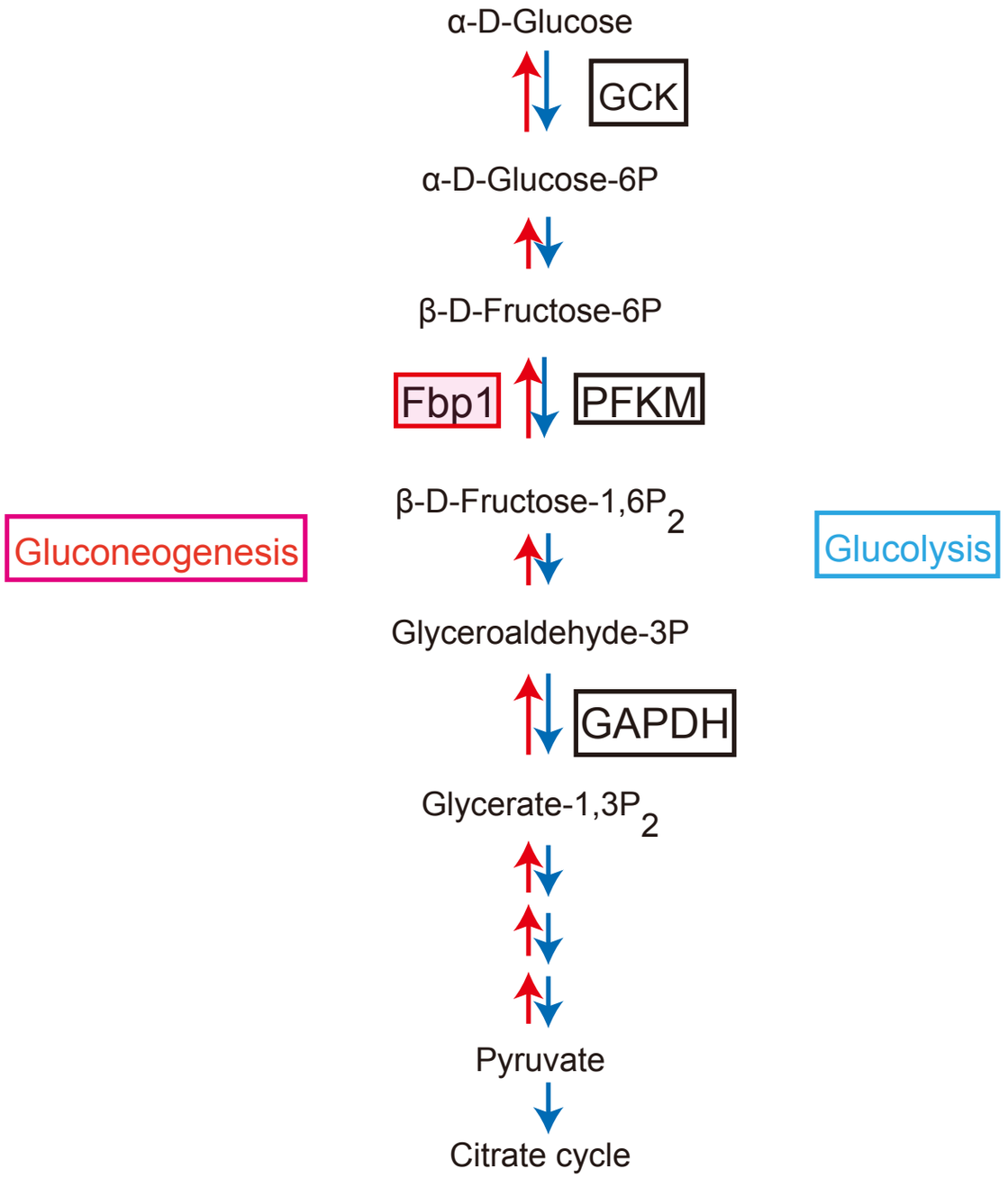

Fig. 1 Gluconeogenesis and glucolysis pathway

Under glucose rich condition, glucolysis pathway indicated in blue is used. However, when glucose starvation is induced, gluconeogenesis pathway is activated to produce glucose from other carbon sources.

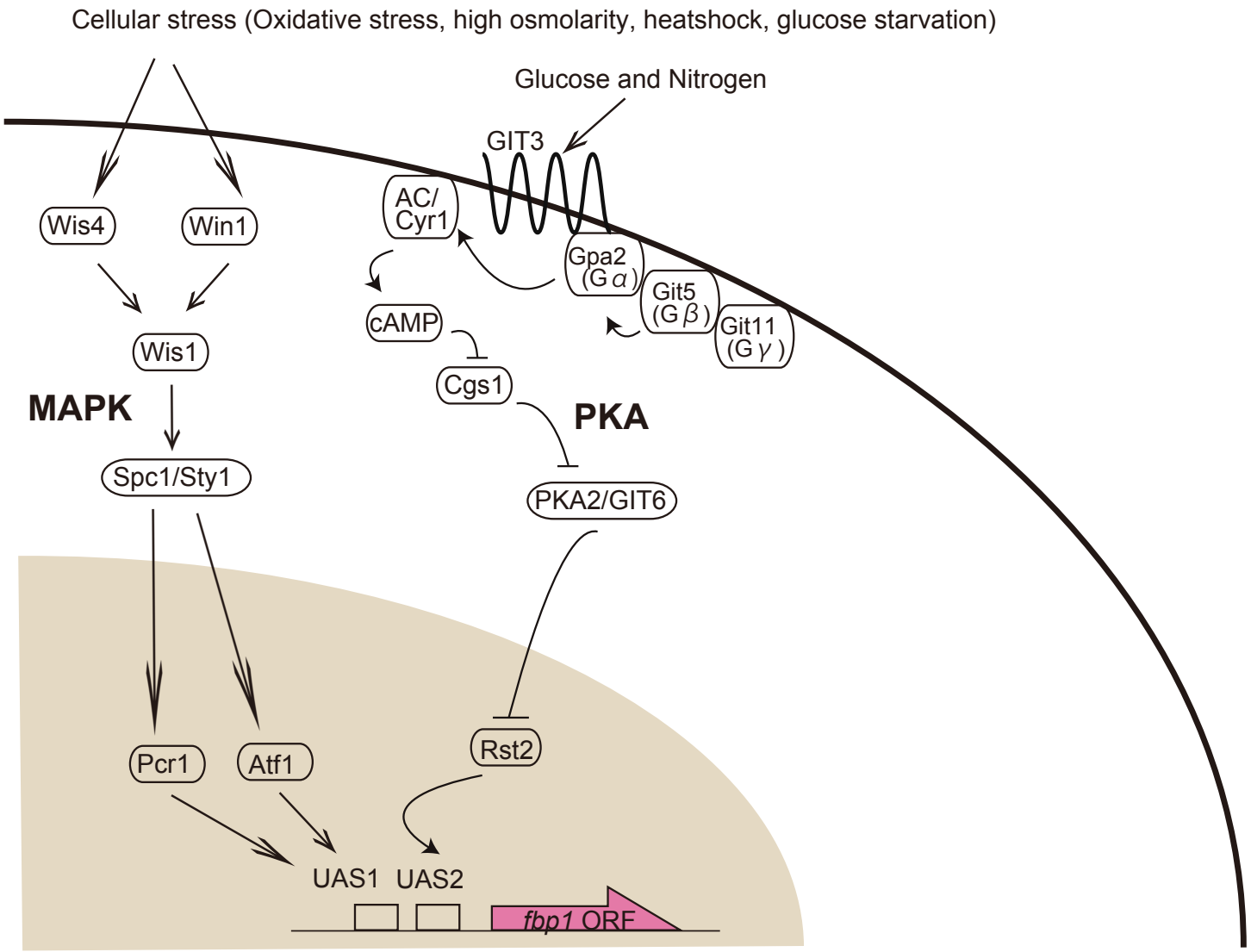

Fig. 2 Signal pathways involved in *fbp1* induction

Cellular stresses activate MAPK pathway and transcription factors Pcr1 and Atf1, and activated Pcr1-Atf1 bind to UAS1. Glucose and nitrogen starvation activate Rst2, which binds to UAS2.

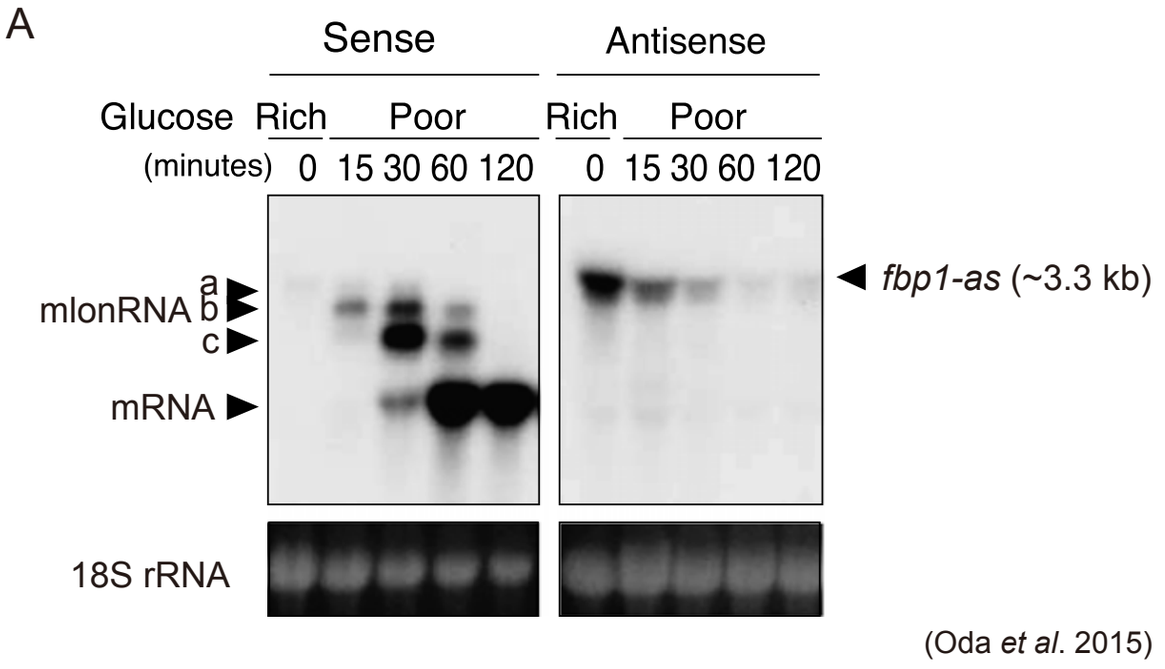

(Oda *et al*. 2015)

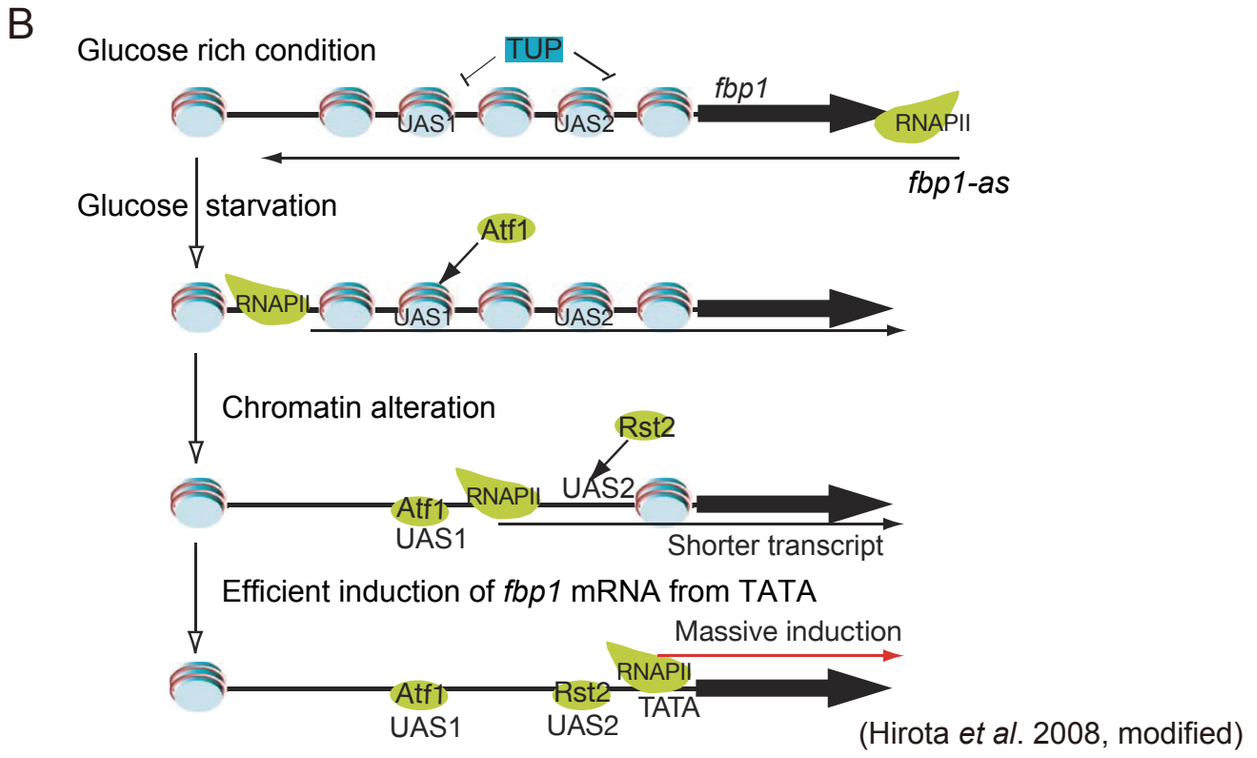

(Hirota *et al*. 2008, modified)

Fig. 3 Sense and antisense RNAs from *fbp1* locus

A. Wild type cells were shifted from glucose rich (6%) to poor (0.1%) medium to induce glucose starvation, and then cells were collected as indicated time points. Top panels: Northern blot analyses using a strand-specific probe against sense (Left) and antisense (Right) RNAs. Bottom panels: 18S rRNA as a loading control.

B. Scheme of transcription around *fbp1* locus. Under glucose rich condition, *fbp1-as* is transcribed and *fbp1* sense RNAs are repressed by TUP11/12 corepressors. After glucose starvation, Atf1 and Rst2 binds to UAS1 and UAS2 region respectively to induce sense mlonRNAs, which lead to chromatin remodeling and induction of *fbp1* mRNA.

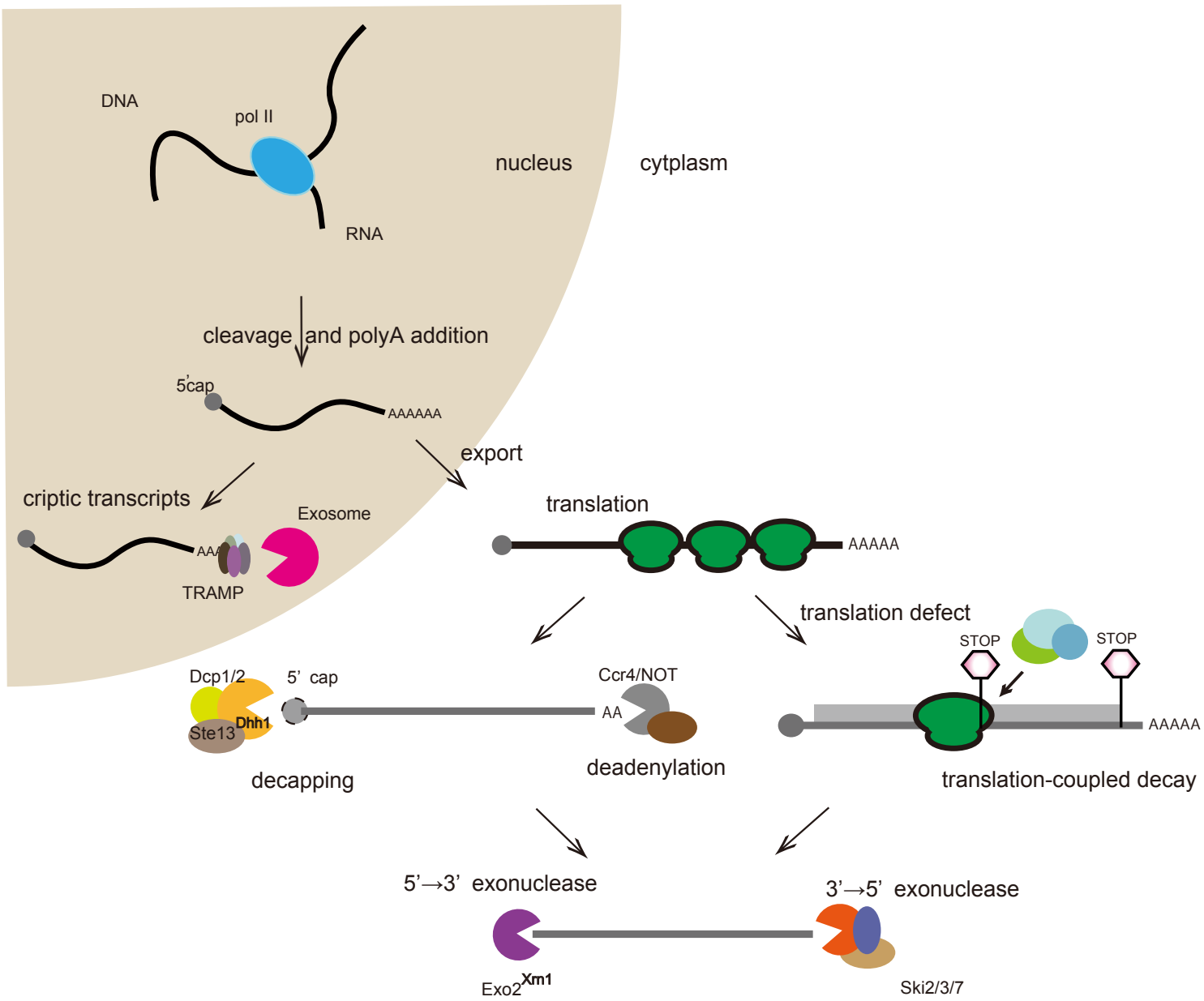

Fig. 4 RNA degradation pathway in the cell

Some of the RNAs transcribed in the nucleus are degraded by the nuclear exosome. RNAs exported to cytoplasm are translated and degraded either from 5' or 3' end. Decapping followed by 5' to 3' exonuclease Exo2 is responsible for 5' to 3' degradation. On the other hand, polyA shortening followed by 3' to 5' exonuclease Ski complex (Ski2/3/7) is responsible for 3' to 5' degradation. When translation defect was caused by ribosome stalling, translation-coupled decay pathway detect it and this lead to degradation of aberrant transcripts.

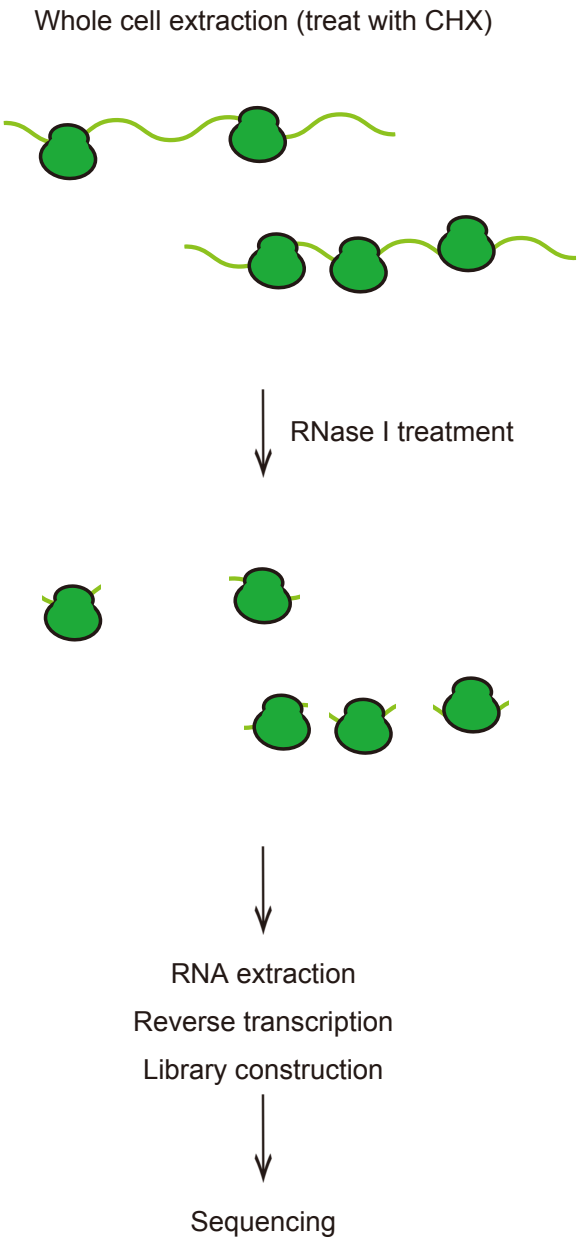

Fig. 5 Scheme of ribosome profiling (ribo-seq)

Whole cell extracts treated with cycloheximide (CHX) were treated with RNase I to degrade RNAs that were not protected by ribosomes. RNAs evade from RNase I treatment was then extracted, and reverse-transcribed to generate library for NGS analysis.

Materials and methods

Yeast strains

Yeast strains used in this study are listed below. Deletion strains are obtained by knocking out the target region by homologous recombination with a construct containing a hygromycin B or Kanamycin resistance cassette. For the TATA mutant strain, the upstream region of *fbp1* was first deleted by *ura4* and then the region was swapped to the sequence containing TATA mutation.

Name	Genotype	Source
wild type (JY450)	*h90 ade6-M216 leu1-32*	M. Yamamoto
cid14Δ (JT654)	*h90 ade6-M216 leu1-32 cid14::nat*	M. Yamamoto, D. Moazed
upf1Δ	*h90 ade6-M216 leu1-32 upf1::kan*	Galipon *et al.* 2013
rrp6Δ	*h90 ade6-M216 leu1-32 rrp6::hph*	Galipon *et al.* 2013
ski2Δ	*h90 ade6-M216 leu1-32 ski2::hph*	this study
exo2Δ	*h90 ade6-M216 leu1-32 exo2::hph*	this study
fbp1Δ	*h- ade6-M26 leu1-32 ura4-D19 fbp1 Δ(-1338 to +1582)*	A. Oda

Media and cell culture

Compositions of media used in this study were described in the table below. Cells were pre-cultured in YES, followed by overnight culture in YER up to the cell density of ~2×10^7 cells/mL. To induce glucose starvation, cells were shifted from YER to YED medium.

	YES	YER	YED
Bacto yeast extract	5 g/L	5 g/L	5 g/L
Glucose	30 g/L	60 g/L	1 g/L
Glycerol	-	-	3%
adenine	200 mg/L	200 mg/L	200 mg/L
leucine	200 mg/L	200 mg/L	200 mg/L
histidine	200 mg/L	200 mg/L	200 mg/L
uracil	100 mg/L	100 mg/L	100 mg/L

RNA purification

Total RNA was extracted using the hot acid phenol procedure as described in (Galipon *et al.* 2013). Briefly, frozen samples were re-suspended in 250 µL of 65ºC beads buffer (75 mM NH_4OAc; 10 mM EDTA, pH 8.0), and transferred to pre-heated tubes with 200 µL of acid washed beads, 25 µL of 10% SDS, and 300 µL of Acid Phenol:Chloroform pH 4.5 (Thermo Fisher Scientific), and incubated for 5 min with three times of 1 min vortex, followed by 10 min incubation at 65ºC. Then tubes were mixed vigorously for 1 min, and centrifuged at 16,000g at room temperature. Supernatant was then transferred to new tube and 200 µL of beads buffer and 400 µL of Chloroform:Isoamyl Alcohol

(Sigma-Aldrich) and mixed briefly. The tubes were centrifuged for 15 min at 4ºC, then supernatant was transferred to new tube containing 7.5 M NH_4OAc (final 0.51 M) and 1.5 volumes of 2-propanol, and centrifuged at 20,400 g for 30 min at 4ºC. The pellet was once washed with 70 % ethanol and dried up in a vacuum hood (TOMY). The pellet was then re-suspended to RNase-free water. RNA concentrations were measured using Nanodrop™ RNA-40.

Northern Blotting and Hybridization

For sense strand RNA detection, 10 µg of total RNA were used for Northern blot. For antisense RNA detection (*fbp1-as* and *per1-as*), 20 µg of total RNA per lane was used, as their signals were weak compared to their sense RNAs. Hybridization and strand-specific probe preparation were conducted as described in (Oda *et al*. 2015). For detection of *per1* mlonRNA and *per1-as,* PCR-amplified DNA templates (primers are listed below) were *in vitro* transcribed with [α^{32}P-CTP] by the Riboprobe system (Promega) (for *fbp1* 3'region, *per1* mlonRNA and *per1-as*) to prepare riboprobes, or were randomly primed by the Random Primer DNA Labeling Kit Ver.2.0 (TaKaRa) to detect *per1* mRNA.

fbp1 3'region	TAATACGACTCACTATAGGTTGGAAGTAAACATGAAGTCGAG
	CTTGTCTACAGTCAGGATTTGGA
SPNCRNA934.1	CAACAGCAAGAAGGGGAGAG
	TAATACGACTCACTATAGGAATCGAGCATTTCACCAAGG
per1 mlonRNA	ATATCGGTTTTTCCGTGCAG
	TAATACGACTCACTATAGGGAAGGGTAAGCCGAGACACA
per1	CGCATCTTGCATTATTTCACC
	ACGGGTTTGAAGTCGCTAAAAAAC

CAP-immunoprecipitation (CAP-IP)

Anti-CAP IP experiment was performed as described elsewhere (Galipon *et al.* 2013), using 150 µg of total RNA and an anti-methylguanosine antibody.

Poly(A) purification

200 µg of total RNA was incubated with oligo-dT beads (Dynabeads® mRNA direct™ kit, Invitrogen) at room temperature for 15 min. After removing the supernatants, 10 µL of elution buffer (10 mM Tris-HCl, pH 7.5) was added. The mixture was incubated at 85ºC for 10 min to elute poly(A)-tailed RNAs, and the remaining beads were further eluted with lysis buffer and then combined altogether, followed by another round of the above-described incubation and elution cycles.

Strand-specific reverse transcription and real-time quantitative PCR (RT-qPCR)

Total RNA extracted from cells as described above was used according to the manufacturer's protocol. Briefly, 1 µg of total RNA was digested with gDNA Eraser enzyme for 2 min at 42 ^{o}C, using PrimeScript® 1st strand cDNA Synthesis Kit (TaKaRa). Primers used for RT-qPCR of *fbp1-as,* and mRNAs of *srp7* and *tub1* are listed below. The qPCR experiments were done as decribed previously (Takemata *et al*. 2016).

RT	*fbp1-as*	AGCAGAGTTGGTAAATCTCATTGG	
	tub1	TCGTTTGGAATTCTGCCAAAT	
	srp7	AGGTGAATCCCATCGCTATCG	
qPCR	*fbp1-as*	AGCAGAGTTGGTAAATCTCATTGG	GTTCATCGCCAGTGGAATTGAC
	tub1	TCGTTTGGAATTCTGCCAAAT	TCTTCCATCACCGCCTCTCT
	srp7	AGGTGAATCCCATCGCTATCG	CTTCGTGGCAACTGGCAGTTA

3'-RACE experiments

To identify the 3' termini of *fbp1-as*, 50 ng of poly(A) purified RNAs were processed by FirstChoice® RLM-RACE kit (Ambion). The supplied 3'-RACE adapter was used for the first strand cDNA synthesis. To avoid non-specific products, nested PCR was conducted. The prepared cDNA was further analyzed by PCR using the supplied 3'-RACE outer primer and *fbp1*-specific outer primer (am51). The PCR product was then used as a template in a second PCR using the 3'-RACE inner primer and *fbp1*-specific inner primer (jg101 or jg110). PCR

products were then cloned into pCR®2.1-TOPO® vector (Invitrogen) for sequencing.

outer primer (am51)	CTTGTCTACAGTCAGGATTTGGA
inner primer (jg101)	CGTTCGACTTCATCGCAGTA
inner primer (jg110)	TGTATCCTAAAACATTACTTGAAAACA

Half-life measurements

To stop RNA synthesis, transcription inhibitor 1,10-phenanthroline monohydrate (Sigma-Aldrich) was added to the culture at a final concentration of 250 mg/L (Galipon *et al.* 2013). Samples were analyzed at indicated several time points after the addition of inhibitor.

Single molecular FISH (smFISH)

smFISH was performed as described in (Heinrich *et al.* 2013). Briefly, 5 mL of cultured cells (~2×10^7 cells/mL) were fixed with final 4% of paraformaldehyde for 30 min at room temperature. After fixation, cells were digested with spheroplast buffer (1.2 M sorbitol, 100 mM $KHPO_4$ at pH 7.5, 20 mM vanadyl ribonuclease complex and 20 µM mercaptoethanol) with 1% 100T Zymolyase (Nacalai tesque) at 30ºC until 40-60 % of the cells were digested (checked under microscope). Digested cells were centrifuged and washed three times with buffer B (1.2 M sorbitol, 100 mM $KHPO_4$ at pH 7.5, at 4^{o}C). Thereafter, the pellet was suspended with PBS containing 0.01 % Triton X-100 for 20 min by rotating at 30 ºC, washed three times with buffer B, and resuspend the pellet with buffer B and

kept on ice while preparing FISH probes. Probes coupled to the Quarsar 570® Dye were designed using Sterallis® Probe Designer version 4.0 (Primers used for smFISH were listed below). For one reaction, 0.15 µL of 25 µM of FISH probes were mixed with 4 µL of 1:1 mixture of yeast tRNA and salmon sperm DNA. Probe mix was dried in a warmed vacuum chamber. Then 50 µL per reaction of buffer F (20 % formamide,10 mM $NaHPO_4$ at pH 7.0) was added to the dried probes and denatured at 95ºC for 3 min. 50 µL per reaction of Buffer H (4x SSC, 4 mg/ml BSA (acetylated) and 20 mM vanadyl ribonuclease complex) was added to the probe mixtures. Then probes were mixed with cells at 37ºC overnight with rotating. Cells were washed with pre-warmed 2x SSC (saline sodium citrate, 0.3 M NaCl, 30 mM trisodium citrate) containing 10 % formamide at 37ºC, followed by twice wash with 2x SSC containing 0.1 % Triton and 1x PBS, respectively. Cells were incubated in PBS containing 0.1 mg/ml DAPI (4', 6-diamidino-2-phenylindole) then washed with PBS and mounted on slide glasses. Fluorescence microscopic images were obtained with an EM-CCD camera (Cascade II, Photometrics, Tucson, AZ)-equipped inverted microscope (IX-83, Olympus) with a 100X oil-immersion objective lens (UPLAN SApo NA 1.4, Olympus), with insertion of an intermediate 1.6X magnification module into the optical path. Image acquisition and 2D deconvolution were performed using the Metamorph software (Molecular Devices, Silicon Valley, CA). Each acquisition consists of 15 gray-scale 16-bit images in steps of 200 nm along the Z-axis. For noise reduction, a two-dimensional Laplacian of Gaussian filter was applied to

each slice. FISH-quant (Mueller *et al.* 2013) version 2d was used for counting *fbp1-as* positive cells. The outline of cells was manually defined and batch-processing was performed. The threshold was set by amplification and the pixel size of the detected signals as described in the manual of FISH-quant. Detected signals were double-checked manually.

sequence (5’-3’)
ccgtaaagtccaaatcctga
acctatttttcagaggacgt
acttatggttgacagttgca
acatggatctccaattaggt
ttcctagttctttgaagtcc
agcagtatttggcttggaag
ggaggtattgcggtaaacga
ggccttccttgttgaacaag
gcttatccatgctcaaaagg
cattctttatggtgggttgt
gttctatggtcgccgatatg
aaccatactctgctcgatac
ctcgttttattgctcatctc
gagggttacactgcattttg
catcttgacccatcgaaaca
cttggacactgatattggcg
acaggtcatcgtgtcaatgg
gctggctatactatgtatgg
gtcttaaggcctggtaaaga
cagtcaaggcgatattagcg
gtatctataaactgcgaccc
gtgttagtgtaggtaccata
atggctcttccaacattgac
ttgatagcaacggttcctat
gaagaggaggatcttatcgt
gctgcaaactcatcgttagt
actgcgatgaagtcgaacgg
tcaattccactggcgatgaa
atctcattggtttatcggga
caccattcgtaaagcagagt
tcagcttcaaattcatcgcc
tggggaattgtcattactgc
ccttgcattattcaagaggc
cgccgatacaatcagaagca
ctcctttattttgcaggaac
tcgacactgacattgtcaca

Fractionation of polysomes

50 mL of YER culture (~2×10^7 cells/mL) was centrifuged, and the cell pellet was stored at -80ºC. The pellet was ground in liquid nitrogen with a pestle and mortar. Then cell powder was collected and thawed on ice for 30-60 min followed by the addition of 0.5 mL Lysis buffer (20 mM HEPES-KOH, pH 8.0, 2 mM magnesium acetate, 100 mM potassium acetate supplemented with 0.05 U/µL RNasin Plus (Promega), EDTA-free Roche complete protease inhibitor cocktail) containing 0.1 mg/mL cycloheximide. The EDTA-treated samples were suspended in 0.5 mL Lysis buffer containing 30 mM EDTA instead of cycloheximide. To eliminate cell debris, the slurry was centrifuged three times. RNA concentration in the supernatant (whole cell extracts) was estimated by Nanodrop RNA-40, and 500 ng of whole cell extracts was deposited on a linear sucrose gradient (15–60 % sucrose; 50 mM Tris–HCl, pH 8.5, 25 mM potassium chloride, 10 mM magnesium chloride) prepared by Gradient Master (Biocomp Inc.). The gradients were centrifuged 4ºC, r_{max} = 231,000 *g*, for 2.5 hours using a SW40 rotor in an ultra-centrifuge (CP70MX, Hitachi-koki) and fractionated using Piston Gradient Fractionator (Biocomp Inc., 300 µL/fraction; 34 fractions). RNA from each fraction was extracted and analyzed as described previously (Galipon *et al*. 2013). Total RNA controls were extracted from whole cell extracts.

Mapping and Data analysis

Ribo-seq and the corresponding RNA-seq data of *S. pombe* under glucose-rich conditions (Subtelny *et al*. 2014) was downloaded from GEO (GSE52809). RNA-seq for glucose starvation was from Oda *et al*. 2015 (DRA002273). Reads were aligned to the *S. pombe* genome (ASM294v2.19) using Bowtie version 1.0.0.

Results

SECTION (I) Characterization of *fbp1* antisense lncRNA (*fbp1-as*)

(1.1) *fbp1-as* possesses a 5'cap and poly(A) tail

It has been demonstrated that many lncRNAs are transcribed by RNA polymerase II (RNA pol II) and are processed co-transcriptionally to harbor a 5' 7-methylguanosine (m_7G) cap structure and a 3' polyadenylation (poly(A)) tail (Bentley 2005; Berretta & Morillon 2009). Therefore, I checked whether or not *fbp1-as* has a 5' cap and a 3' poly(A) tail. The existence of a 5'-cap structure was analyzed by immunoprecipitation with an anti-5'-cap antibody (cap-IP). Fig. 6A indicates that *fbp1-as*, as well as the positive control *tub1* mRNA, was efficiently immunoprecipitated with an anti-5'-cap antibody, while the *srp7* transcript (RNA polymerase III-dependent transcript) was not. These results indicate that *fbp1-as* harbors a 5'-cap structure. I also tested the presence of a poly(A)-tail in *fbp1-as* using oligo-dT-conjugated magnetic beads, and confirmed that *fbp1-as* has a poly(A) tail (Fig. 6B).

To determine the position of 3'-termini and poly(A)-tails of *fbp1-as*, I employed the 3'-rapid amplification of cDNA ends (RACE) method. Although the majority of *fbp1-as* were terminated at the upstream 5'-untranslated region (UTR) of sense strand *fbp1* mRNA (Fig. 7A, black bars), I detected short poly-adenylated transcripts terminated within the 3'-UTR of *fbp1* mRNA (Fig. 7A, gray bars). This suggests that *fbp1-as* transcription may sometimes abort soon after transcriptional initiation. The shorter transcripts corresponding to gray bars

in Fig. 7A were hardly detect by conventional Northern blot using probes against *fbp1* 3'UTR (Fig. 7B). I hereby focused on the largest antisense RNA (~3.3 kb), which is assumed to be representative *fbp1-as* kinetics.

(1.2) Stability of *fbp1-as*

Previous reports have demonstrated that aberrant transcripts are relatively unstable due to degradation by RNA quality control systems either in the nucleus or in the cytoplasm (reviewed in Parker 2012). Non-coding RNAs have been shown to be recognized as such aberrant unstable transcripts, since they lack long open reading frames (ORFs). It is thus likely that *fbp1-as* is also degraded quickly by RNA quality control systems.

I first examined the stability of *fbp1-as* in wild type cells. To measure the half-life of *fbp1-as*, RNA pol II-dependent transcription was inhibited by the addition of 1,10-phenanthroline in the glucose-rich culture (final 250 ng/μl), according to the method by Galipon *et al.* 2013. After adding the inhibitor, cells were collected at indicated time points. RNAs were then extracted and analyzed by Northern blot using a strand-specific probe which covers *fbp1* ORF (+14 to +1285, nucleotide positions relative to the first A of the initiation codon for *fbp1* ORF) to quantitatively monitor the decay process.

I found that the half-life of *fbp1-as* was 14 ± 2 min in wild type cells (Fig. 8), which is substantially shorter than sense-strand transcripts, such as *fbp1* mRNA ($t_{1/2}$ > 2 hours) and mlonRNA ($t_{1/2}$ ≈ 30 min) (Galipon *et al.* 2013). It should be

also noted that the half-life of *fbp1-as* is much shorter than the previously published median of *S. pombe* non-coding RNA half-lives (30.5 min) (Hasan *et al.* 2014). These data suggest that *fbp1-as* may be destabilized possibly by degradation by RNA quality control systems.

(1.3) Localization of *fbp1-as*

Next, I examined the intracellular localization of *fbp1-as* by single-molecule fluorescence *in situ* hybridization (smFISH) in wild type cells. In this method, about 30-40 probes are designed to amplify the signals to detect individual RNA molecules (Raj *et al*. 2008). I used 36 probes in total for hybridization to *fbp1-as* (Fig. 9A, see also Materials and Methods). The results of smFISH analysis revealed that the majority of wild type cells in an asynchronous culture do not express *fbp1-as,* and *fbp1-as* was expressed on average at 0.58 copies per cell (39 *fbp1-as* foci in 25 cells out of 67, Fig. 9B and C). As a negative control, *fbp1* region (-1338 to +1582) deleted strain (*fbp1Δ*) was used and only 2 nonspecific foci were observed in the negative controls lacking *fbp1-as* (n = 53) (Fig. 9B, see also Fig. 10). Moreover, most *fbp1-as* foci were detected in the cytoplasm (26 out of 39 foci, arrowhead in Fig. 9B, and see also Fig. 10, 11, and 12). These data indicate that *fbp1-as* expression is rare and that *fbp1-as* mainly localizes in the cytoplasm.

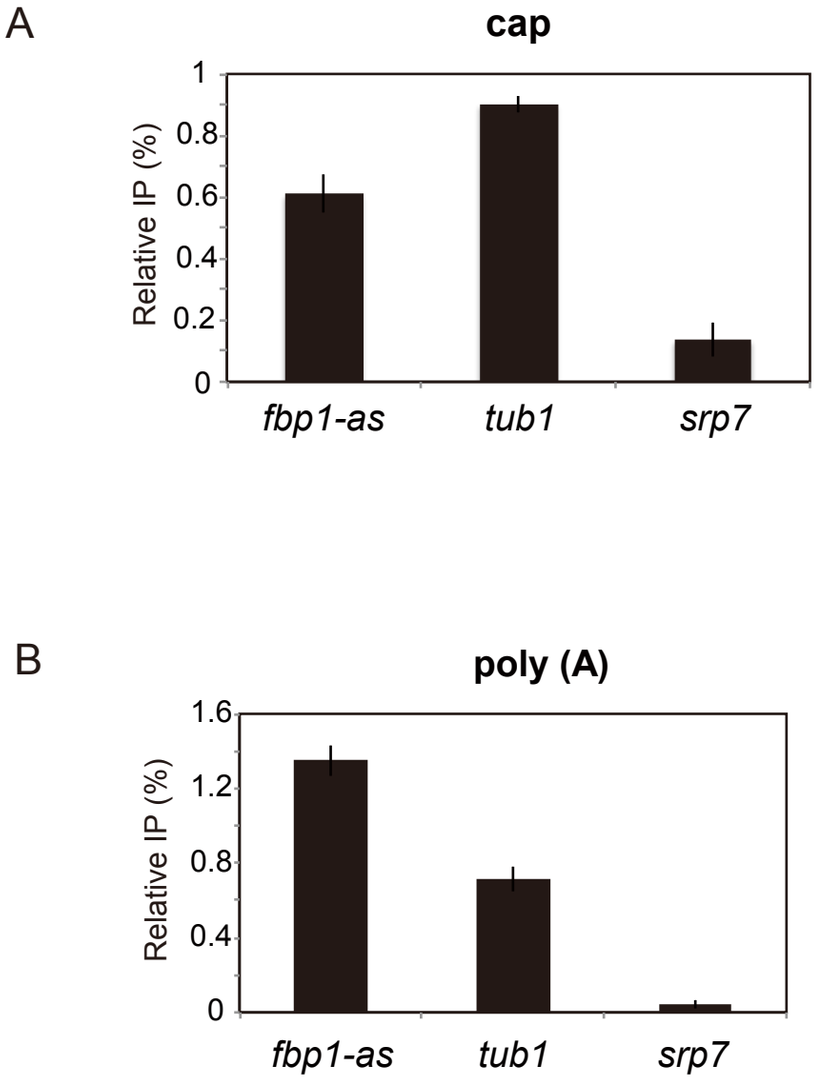

Fig. 6 *fbp1-as* has both 5'cap structure and poly (A) tail.

A. Immunoprecipitation (IP) assays using anti 5'-cap antibody (m3G/m7G-specific antibody). IP efficiency relative to the input (2 biological replicates) was estimated by RT-qPCR assay. Vertical bars represent standard deviations. Note that *fbp1-as* and *tub1* mRNA were 5'-capped, whereas *srp7* RNA was not.

B. Antisense RNA has poly(A)-tail. Poly(A)+ RNA was enriched using Dynabeads® mRNA direct™ kit (Invitrogen). The enrichment relative to the input level was estimated by RT-qPCR. Mean value of 2 biological replicates and standard deviations are shown.

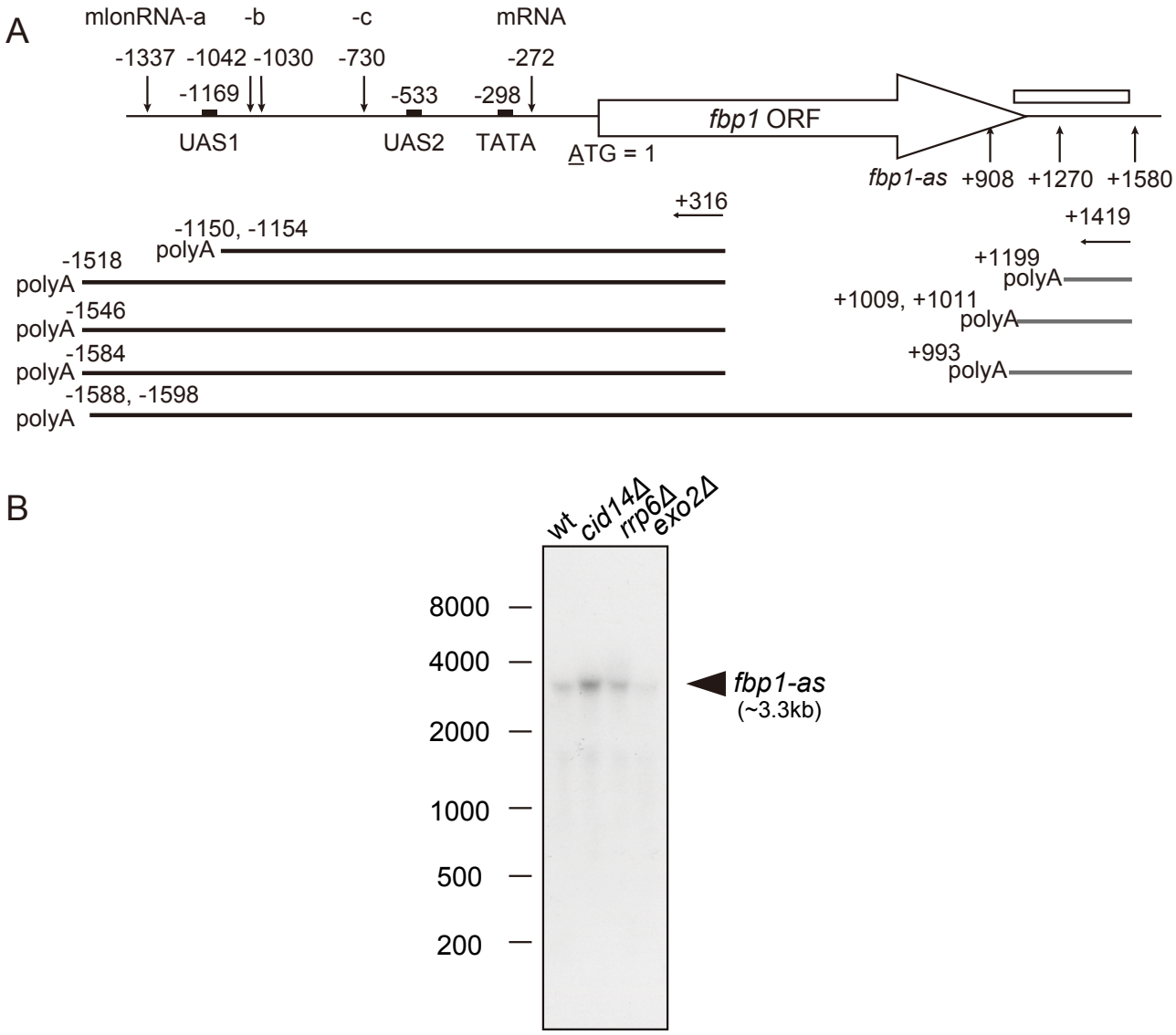

Fig. 7 3'-RACE analysis revealed 3' termini of *fbp1-as*

A. The 3' termini of *fbp1-as* were determined by 3'-RACE cloning followed by DNA sequencing. Previously identified transcriptional start sites for sense *fbp1* mlonRNAs (a,b, and c), mRNA, and *fbp1-as* are indicated by vertical arrows along with the nucleotide positions relative to the first A of the initiation codon for *fbp1* open reading frame. Known transcription factor binding sites (UAS1 or UAS2) and the TATA box are indicated by black boxes. Horizontal black arrows indicate the position of primers used for the 3'-RACE experiment. The sequenced tracts are indicated in black and gray bars. The location of the probe used for short transcripts (gray bars) detection is shown in an open box.

B. Northern blot using strand-specific probe located in 3'UTR region (indicated in an open box in Fig. 7A). Indicated strains were cultured in glucose rich condition. Only long transcript (~3.3kb) corresponding to black tracts in Fig. 7A was detected, and short transcripts shown in gray bars in Fig. 7A could not dedected even in RNA decay mutants. Note that 3'UTR region of *fbp1* mRNA is AT-rich thus *fbp1-as* signal is weaker than in other figures using probes against *fbp1* ORF region (+14 to +1285).

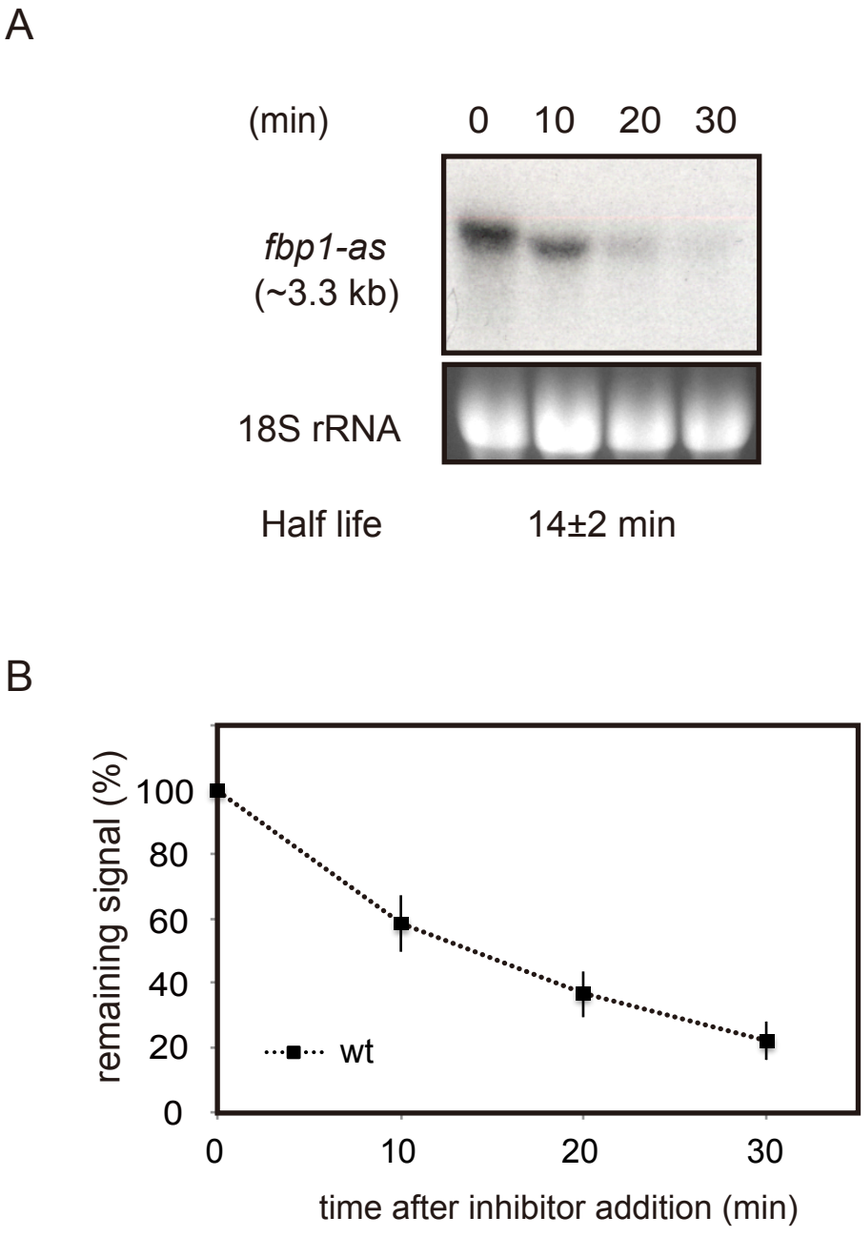

Fig. 8 *fbp1-as* is unstable transcript

A. Half-life of *fbp1-as*. Wild type cells were treated with RNA pol II inhibitor 1,10-phenanthroline (Phe). Top panel: Northern blot analysis using a strand-specific probe which covers around *fbp1* ORF region (+14 to +1285). Time (min) after Phe addition is indicated. Bottom panel: ethidium bromide staining showing 18S rRNA as a loading control.

B. Quantification of the band intensity of the longest type of *fbp1-as* (~3.3kb) in wild type as the remaining signal relative to 0 min (before addition of Phe). Error bars represent the standard deviations of three biological replicates.

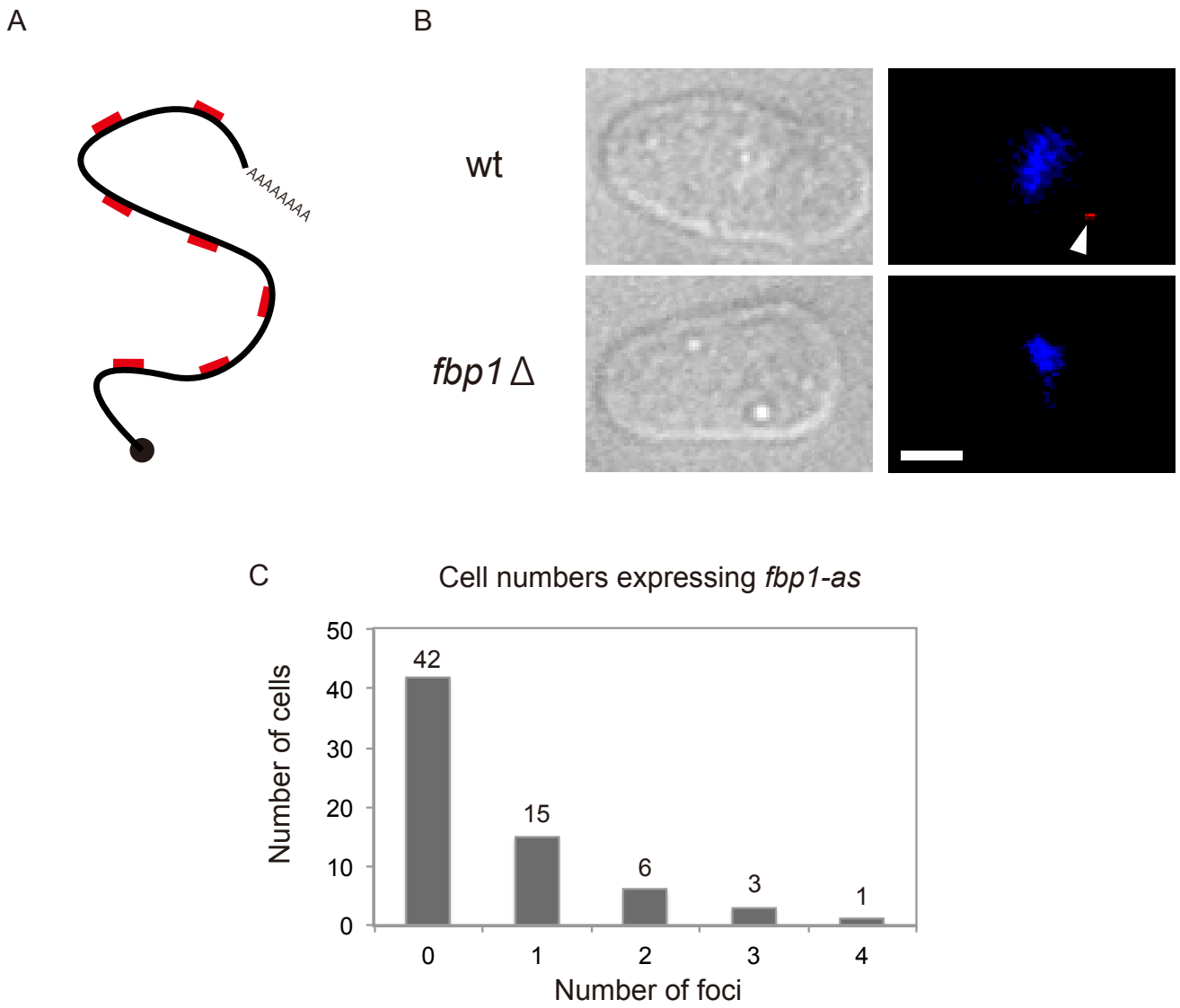

Fig. 9 Single molecule FISH (smFISH) against *fbp1-as*

A. Scheme of smFISH. Total 36 probes were designed to detect *fbp1-as*.

B. SmFISH against *fbp1-as*. Cells cultured in glucose rich medium were fixed and smFISH against *fbp1-as* was performed as described in Materials and methods. The scale bar represents 2 μm. Left panels: phase contrast. Right panels: Z-stacked images of fluorescence images were deconvolved using Metamorph software (see Materials and methods). smFISH and DAPI deconvolved images were merged. An arrowhead indicates a focus (red) of *fbp1-as*. Blue signal is DAPI-stained nuclear DNA. *fbp1*Δ strain lacking the entire *fbp1-as* region (-1338 to +1582) was used as a negative control.

C. The quantification data of (B) in wild type cells (n=67). Number of cells with *fbp1-as* foci are indicated above each bar.

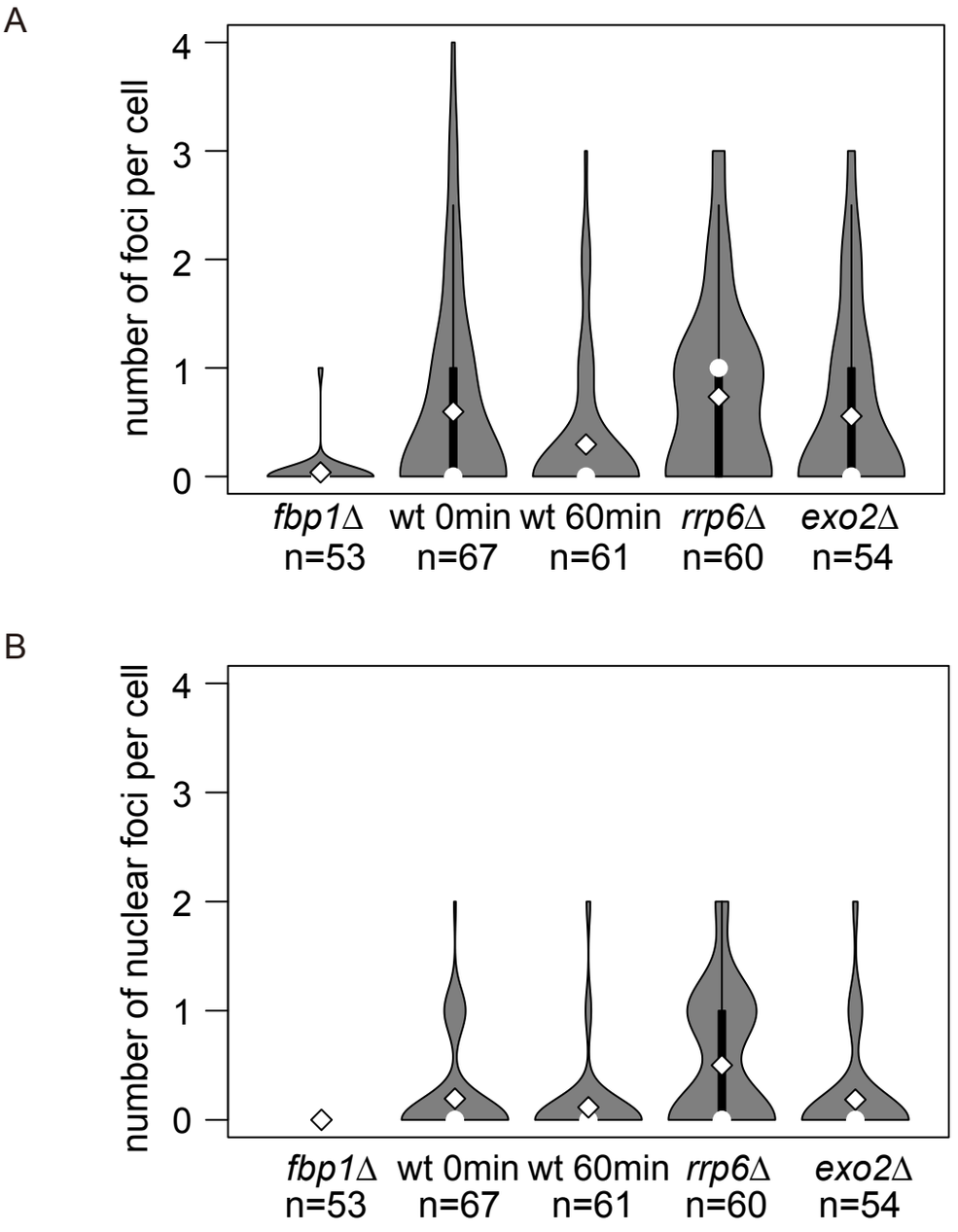

Fig. 10 Localization of *fbp1-as* in various mutants.

A-B. Violin plots showing the relative frequencies of total (A) and nuclear (B) foci per cell. The black vertical bars inside the violin plot correspond to standard boxplots, the white circles represent the median and the white rhombus shapes with black borders represent the mean for each strain. The number of cells in each sample is indicated at the bottom. To confirm whether *fbp1-as* signal was decreased under glucose-starved condition as shown in Northern analysis (Fig. 3), 60min after glucose starvation, wild type cells were collected as 'wt 60min' samples. See also Fig. 11.

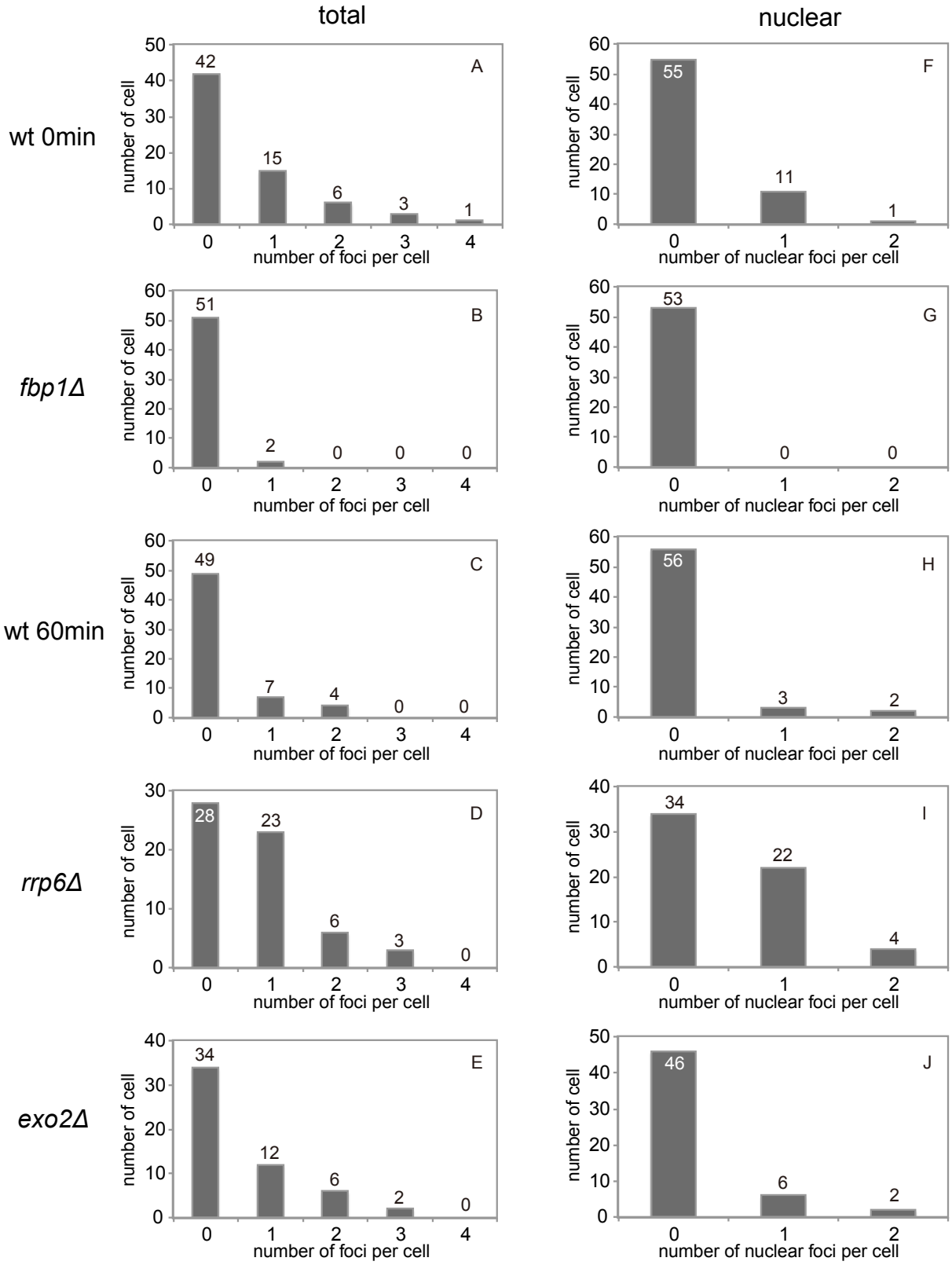

Fig. 11 Number of *fbp1-as* in various mutants.

Histograms for numbers of *fbp1-as* foci in each cell (A-E) or in each nucleus (F-J) of strains indicated on the left side of panels (See also Fig. 10 and Fig. 12). Number of cells with *fbp1-as* foci are indicated above each bar. The data in (A) is the same as in Fig. 9C.

.

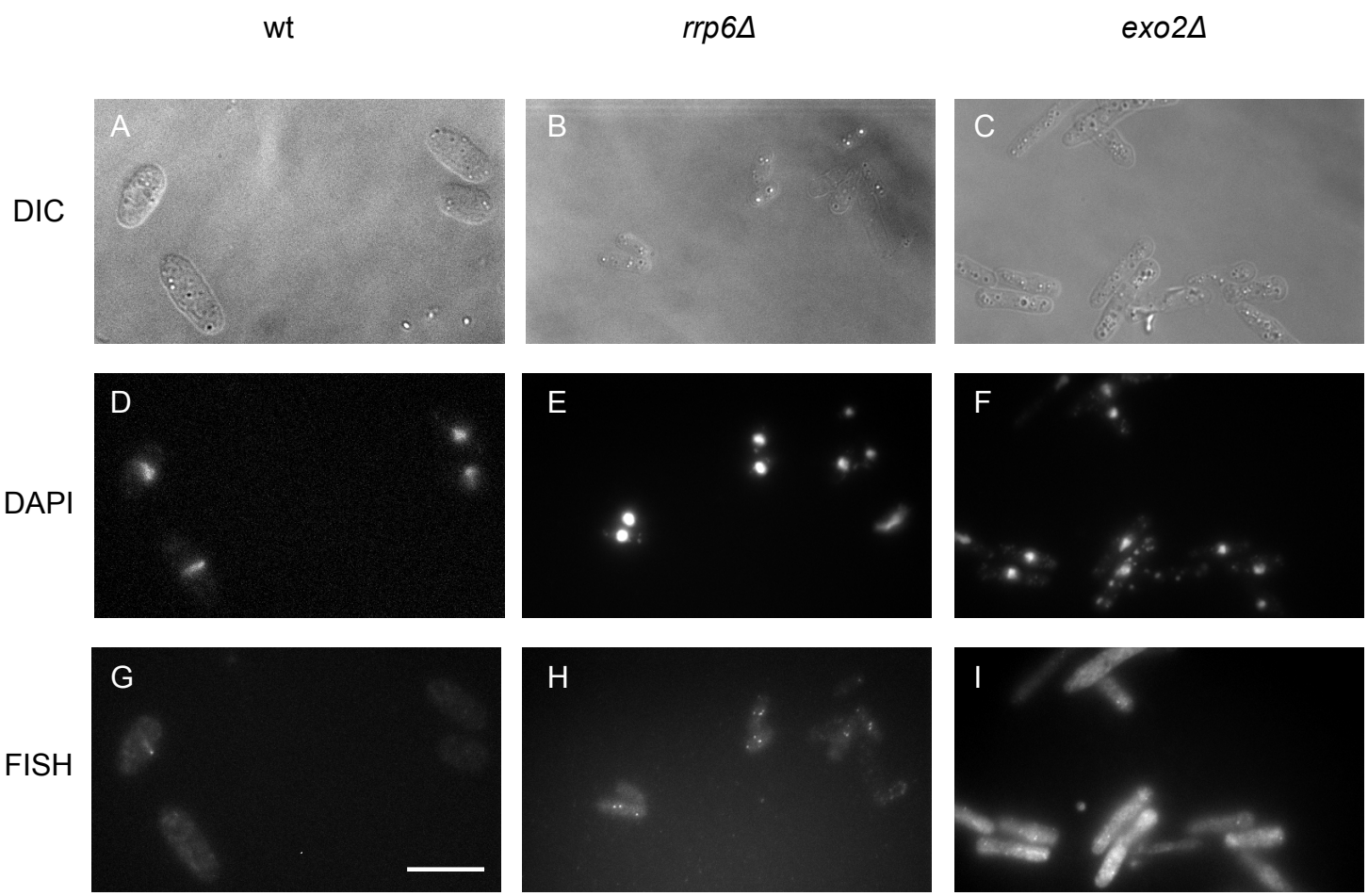

Fig. 12 smFISH data of *fbp1-as* in several mutnts

Raw images of the data in Fig. 10 and Fig. 11. Images of DIC (A-C), DAPI (D-F), and FISH (G-I) of each strains (column wt, *rrp6Δ*, and *exo2Δ*). These images were obtained by projecting Z-stacked images to a single plane with the maximum intensity. The fuzzy cytoplasmic signals in *exo2Δ* cells in (I) are due to non-specific background. The scale bar represents 10 μm.

SECTION (II) Stability control of *fbp1-as*

(2.1) Degradation of *fbp1-as* and localization regulation

Many non-coding RNAs, including CUTs, are prone to degradation by the nuclear exosome (Wyers *et al.* 2005). Therefore, I examined the involvement of Rrp6, the nuclear exosome cofactor, in the decay of *fbp1-as* using the half-life analysis (Fig. 13). I found that the half-life of *fbp1-as* was 4.6-fold longer (64 ± 8 min, p-value = 0.0005) in *rrp6Δ* than in wild type. It should be also noted that the steady-state level of *fbp1-as* in *rrp6Δ* was moderately higher than in wild type (Fig. 14). Since *fbp1-as* is polyadenylated, I also estimated the half-life of *fbp1-as* in a *cid14Δ* deletion mutant. Cid14 is a component of the nuclear TRAMP (Trf4/Air2/Mtr4 polyAdenylation) complex, and is involved in the degradation of some polyadenylated transcripts together with the nuclear exosome (Bühler *et al.* 2008). The data (Fig. 13) indicated that the half-life of *fbp1-as* was 4.3-fold longer (60 ± 11 min, p-value = 0.0020) in *cid14Δ* than in wild type. These results indicate that the nuclear RNA quality control systems are at least partly involved in the decay process of *fbp1-as*.

We previously reported that sense-strand *fbp1* mlonRNA is transcribed from the complementary strand of the *fbp1-as* template in response to glucose starvation. They are also subjected to the nuclear RNA quality control systems, but are nevertheless exported to the cytoplasm (Galipon *et al.* 2013). Therefore,

it is possible that some portion of *fbp1-as* can be exported to the cytoplasm and also targeted to cytoplasmic RNA surveillance systems.

To test this idea, the half-life of *fbp1-as* in *ski2Δ* and *exo2Δ* mutants was examined. Ski2 is included in the cytoplasmic SKI complex, which promotes 3' to 5' RNA degradation. Exo2 is the fission yeast counterpart of budding yeast *XRN1*, which is a conserved 5' to 3' exonuclease in the cytoplasm. Xrn1 degrades RNA byproducts and is a major component of most cytoplasmic RNA surveillance systems. I found that the half-life of *fbp1-as* was largely elongated in *exo2Δ* (> 60min), while less affected in *ski2Δ* (28 ± 1min) (Fig. 15). These results suggest that the fraction of *fbp1-as* that evades nuclear degradation is further subjected to decay from the 5'-end in the cytoplasm.

I also confirmed the presence of *fbp1-as* in the cytoplasm by smFISH using *rrp6Δ* and *exo2Δ* mutants, and found that more *fbp1-as* foci were localized to the nucleus in *rrp6Δ* in comparison to wild type or *exo2Δ* (Fig. 10, 11, and 12). These results are consistent with the notion that majority of *fbp1-as* are quickly degraded by the Rrp6-dependent nuclear decay systems, but some proportion of *fbp1-as* evade such degradation and are exported to the cytoplasm.

(2.2) Cytoplasmic *fbp1-as* can associate with ribosomes

The sequence of *fbp1-as* harbors many small open reading frames (sORF) iniated from AUG: the longest isoform of *fbp1-as* has as many as 89 AUGs, and

30 of them represent the start of sORFs containing at least 20 codons with the termination codons (Fig. 16A). Given that *fbp1-as* is localized in the cytoplasm and has a 5'-cap and poly(A)-tail, it is plausible that *fbp1-as* may interact with ribosomes like mRNAs.

To test this notion, I investigated ribosome association with *fbp1-as* using polysome fractionation followed by Northern analysis. Extracts prepared from wild type cells cultured in glucose-rich medium were fractionated on a sucrose density gradient (see Materials and methods). The RNA concentration of each fraction was estimated by the absorbance at 254 nm, and the representative aliquots were further examined by Northern hybridization using a strand-specific riboprobe for *fbp1-as*. I detected *fbp1-as* in the "heavy density fractions", which correspond to the "multiple ribosome" or "polysome" fractions (see fractions labeled "III" in Fig. 16B). More importantly, these RNA signals disappeared as ribosomes were dissociated by treatment with ethylenediaminetetraacetic acid (EDTA) (Fig. 16C). This data support that *fbp1-as* in the cytoplasm is associated with ribosomes.

I then identified the position of ribosome association on *fbp1-as*, by analyzing the published *S. pombe* Ribo-seq data under glucose-rich conditions (Subtelny *et al.* 2014). The ribo-seq reads were indeed mapped to the *fbp1-as* region (Fig. 17). These data suggest that *fbp1-as* has active sORFs, though whether these sORFs really produce small peptides still remains to be proven.

(2.3) Cytoplasmic decay of *fbp1-as* depends upon the NMD pathway

Given that *fbp1-as* is rapidly degraded and associated with ribosomes (Fig. 17), it is assumed that *fbp1-as* is targeted to the translation-coupled decay systems. I therefore compared the half-lives of *fbp1-as* in the presence or absence of the translation inhibitor cycloheximide (CHX), which is known to inhibit the dissociation of ribosomes from RNAs. I expected that if *fbp1-as* is targeted to translation-coupled decay mechanisms, the half-lives of *fbp1-as* should be substantially affected by CHX. The results in Fig. 18A and B clearly indicate that *fbp1-as* was dramatically stabilized in the presence of CHX ($t_{1/2}$ > 60 min). This suggests that *fbp1-as* is degraded co-translationally.

Nonsense-mediated decay (NMD) is a well-characterized co-translational decay system, known to target RNAs with premature termination codons. The recognition step is triggered by the assembly of the Upf1/2/3 complex which catalyzes RNA degradation (Brogna & Wen 2009). In addition, mRNAs containing multiple sORFs in the 5'-UTR (Gaba *et al.* 2005; Medenbach *et al.* 2011) or mRNAs with long 3'-flanking sequences (Muhlrad & Parker 1999; Kebaara & Atkin 2009) are often targeted to this NMD system. Indeed, *fbp1-as* has many sORFs (Fig. 16A), including an sORF corresponding to the estimated ribosome binding site (Fig. 17, Ribosome, "plus strand"). Probably, anything downstream of this sORF in *fbp1-as* might be recognized as a long 3' flanking sequence in *fbp1-as*.

To evaluate the involvement of NMD in the decay of *fbp1-as* by estimating the half-life of *fbp1-as* in *upf1Δ*, which is deficient in the NMD pathway (Rodríguez-Gabriel *et al.* 2006). I found that *fbp1-as* was markedly stabilized in *upf1Δ* ($t_{1/2}$ = 40 ± 3 min) (Fig. 18). It should be also mentioned that the *fbp1-as* steady-state levels in *upf1Δ* were substantially increased (Fig. 14). These results demonstrate that *fbp1-as* is targeted to the cytoplasmic NMD pathway, and are consistent with degradation of *fbp1-as* by Exo2 (Fig. 15), which is known to be involved in NMD in other organisms (Muhlrad & Parker 1994; Lejeune *et al*. 2003) and in the decay of some non-coding RNAs (Smith & Baker 2015). On the other hand, the NMD-dependent decay of *fbp1-as* in glucose rich condition exhibits a sharp contrast to the decay of *fbp1* sense-strand lncRNAs during glucose starvation, which are totally independent of NMD degradation (Galipon *et al.* 2013).

(2.4) Generality investigation in other stress-responsive antisense RNAs

I then examined whether the above-mentioned features of *fbp1-as* are observed in other stress-responsive lncRNAs that exhibit a reciprocal conversion from antisense to sense transcripts in response to stress. First, I studied the presence of ribosome-protected fragments on known glucose stress-responsive antisense RNAs using publicly available Ribo-seq data

obtained from *S. pombe* cells cultured in glucose-rich conditions (Subtelny *et al.* 2014).

Previously, it was reported that 9 high-confidence loci express sense lncRNAs similar to *fbp1* mlonRNA in response to glucose starvation (Oda *et al*. 2015). Importantly, 5 of them also express antisense transcripts in glucose rich conditions, the expression of which are anti-correlated with the induction of sense strand transcripts upon glucose starvation (Oda *et al*. 2015).

When I investigated Subtelny's Ribo-seq data of *S. pombe* in glucose rich conditions (Subtelny *et al.* 2014), it turned out that 3 loci out of these 5 candidates exhibited clear ribosome occupancy on the antisense RNAs expressed in glucose rich conditions. They are *ght4* (hexose transporter), *SPAC4H3.03c* (predicted glucan 1,4-alpha-glucosidate), and *per1* (plasma membrane aminoacid permease). Among these, only the *per1* locus had strong enough signals to detect by Northern blot (Fig. 19), which is necessary to validate the full-length size of transcripts. Therefore, I hereafter present results obtained for the *per1* locus.

As shown Fig. 19, Northern blot analysis confirmed that *per1* indeed expressed continuous sense and antisense lncRNAs, which are consistent with the Oda's RNA-Seq data (Oda, *et al.* 2015, Fig. 20), The *per1* locus expressed an antisense RNA in glucose rich conditions, while *per1* began to express a low amount of an mlonRNA-like sense transcript as cells were shifted to glucose poor media (Fig. 19 and 20). This mlonRNA-like transcript covered a region

including both the *SPNCRNA.935.1* and *per1* annotations, forming one long continuous transcript. The *per1* antisense RNA (previously annotated as *SPNCRNA.934.1*, hereby referred to as "*per1-as"*), transcribed from the opposite strand of the *per1* mlonRNA template strand, has many sORFs (Fig. 20, open circles). The analysis on the above-mentioned Ribo-seq data indicated that ribosomes interacted with some of these sORFs in *per1-as* (Fig. 21A).

To further confirm whether *per1-as* shares similar features with *fbp1-as*, the half-lives of *per1-as* in wild type and *upf1Δ* (deficient in NMD) cells were measured by treatment with the transcription inhibitor phenanthroline. As seen in *fbp1-as*, the half-life of *per1-as* was relatively short (27 ± 4 min), while a marked stabilization of *per1-as* was observed in *upf1Δ* (131 ± 34 min) (Fig. 21B), suggesting that the NMD pathway is indeed involved in the rapid turnover of *per1-as*.

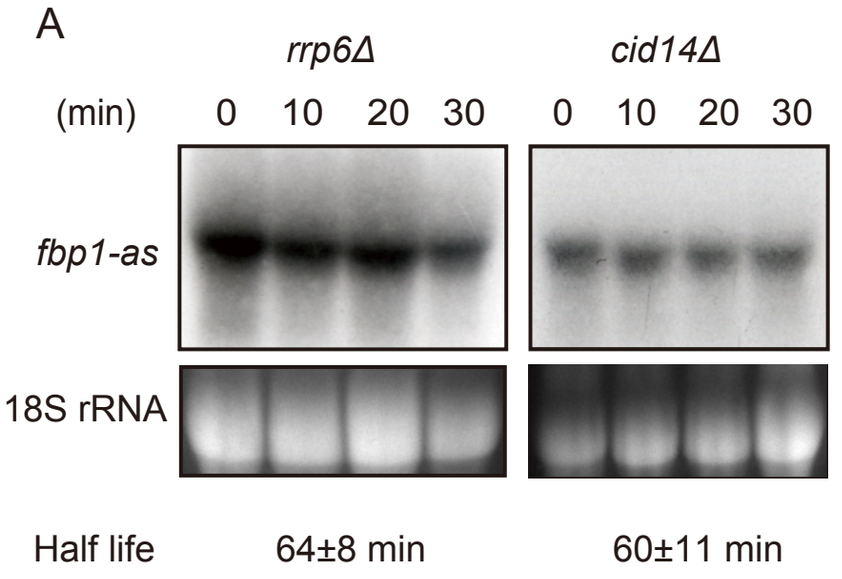

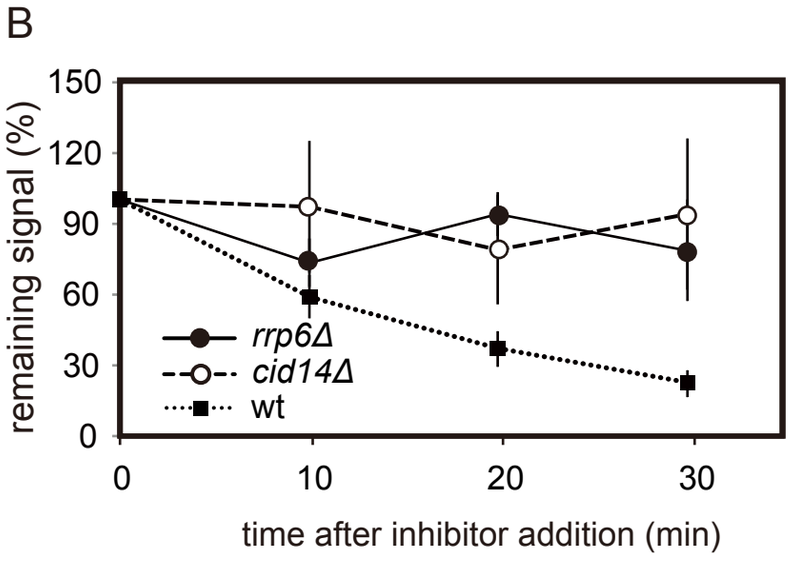

Fig. 13 *fbp1-as* is degraded in nucleus

A-B. Deletion of Rrp6 or Cid14 affects *fbp1-as* stability. (A) Top panels: Northern blots using the same strand-specific probe as in Fig. 8A. Bottom panels: ethidium bromide staining showing 18S rRNA as a loading control. (B) The quantification data of (A). Error bars represent the standard deviations of three biological replicates. Solid, dashed, dotted lines represent *rrp6*Δ*, cid14*Δ*,* and wild type (same data as in Fig. 8B), respectively.

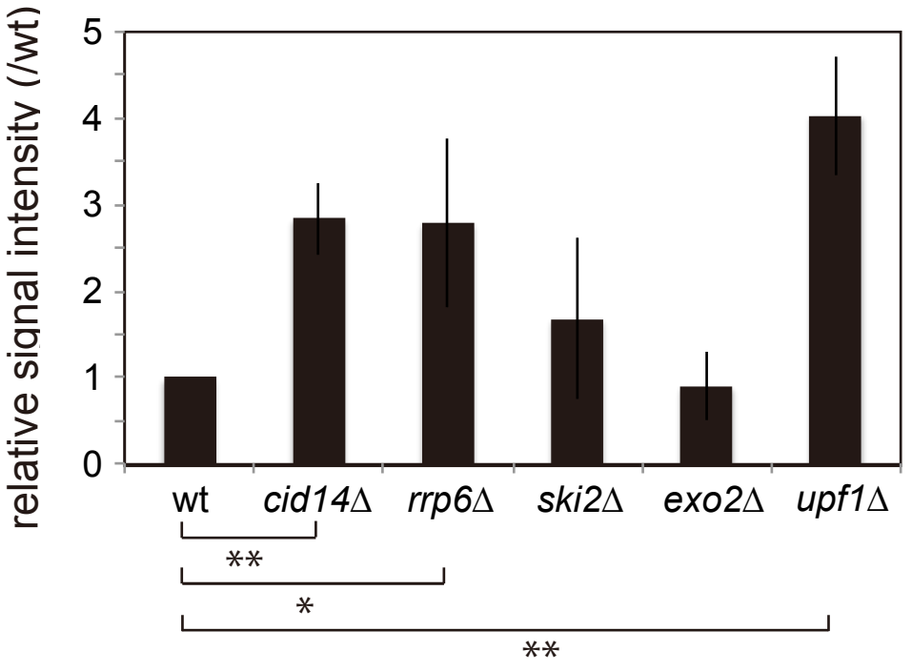

Fig. 14 Steady-state level of *fbp1-as* in various mutants.

Steady-state levels of *fbp1-as* in various RNA decay mutants. Northern blot signals were normalized to ribosome signals. Standard unpaired *t-tests* were carried out in comparison with wild type. The data with error bars (standard deviation) are the average of three replicates.

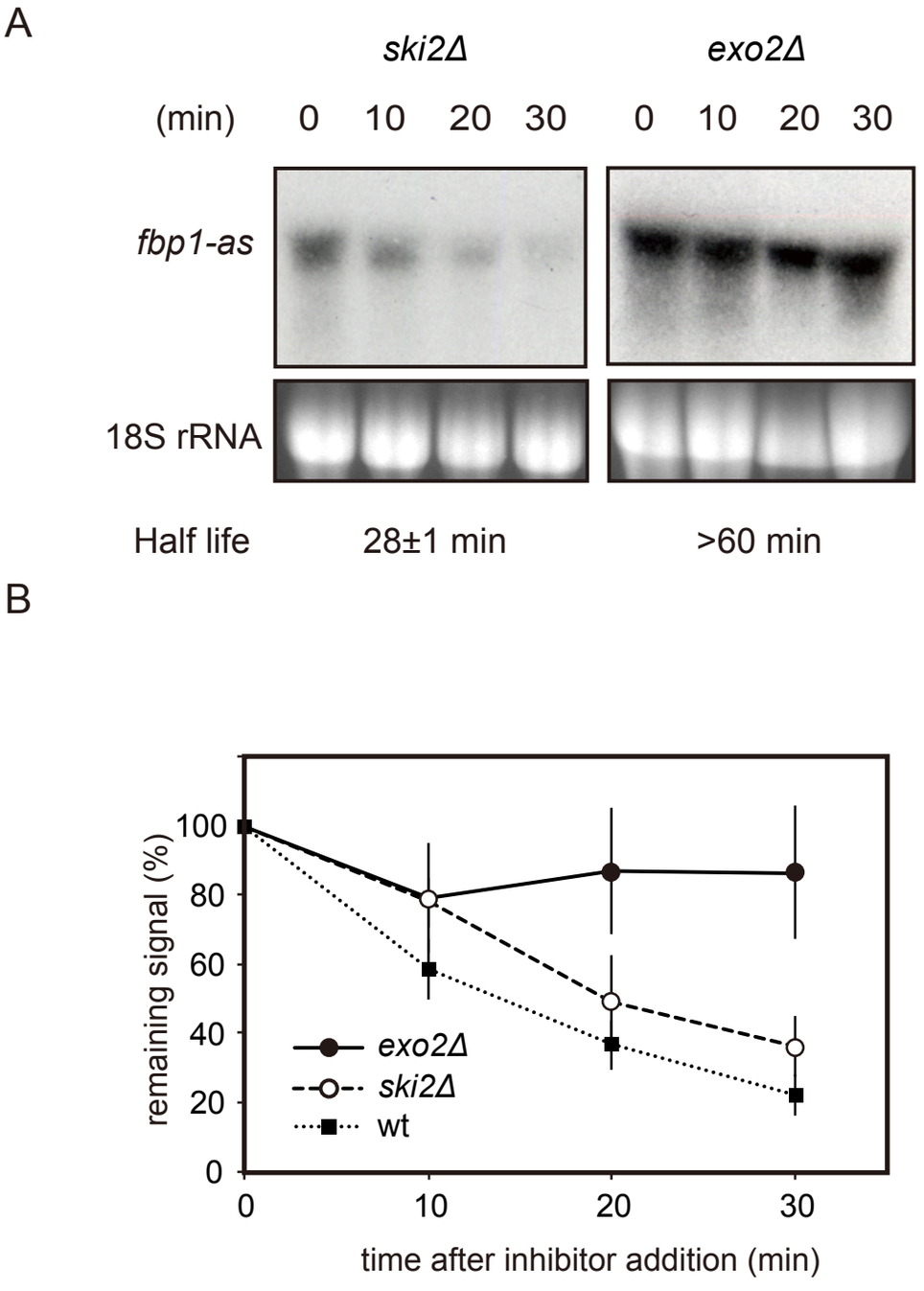

Fig. 15 *fbp1-as* is degraded both in nucleus and in cytoplasm

A-B. Effect of the deletion of Ski2 or Exo2 on *fbp1-as* stability. (A) Northern blot with the same strand-specific probe used in Fig. 8A. (B) The quantification data of (A). Error bars represent the standard deviations of three biological replicates. Solid, dashed, dotted lines represent *exo2*Δ, *ski2*Δ, and wild type (same data as in Fig. 8B), respectively.

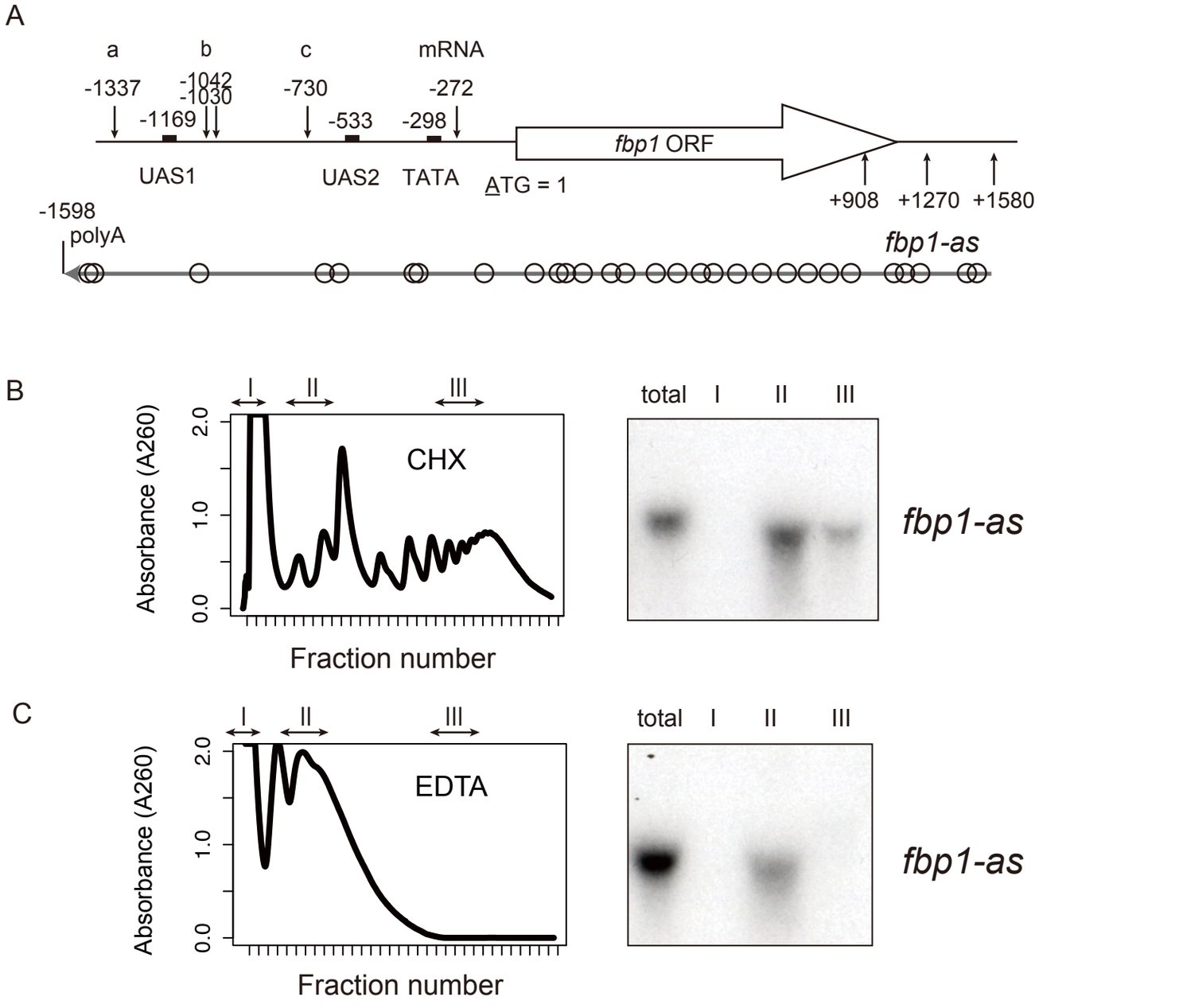

Fig. 16 *fbp1-as* has multiple small ORFs and localizes to polysomes

A. Open circles represent small ORFs with more than 20 codons, including the termination codon. The top part is the same as in Fig. 7.

B-C. Polysome fractionation confirms *fbp1-as* association with ribosomes. Left panels: UV absorbance along the sucrose gradient. Left right arrows I, II, and III represent free, 40/60/80S, and polysome fractions, respectively. Right panels: Northern blot analysis of polysome fractionated samples using strand-specific probes to detect *fbp1-as*. Total RNA controls were extracted from 20 µg of whole cell extracts. (B) Cell extracts were treated with cycloheximide (CHX) to prevent ribosome dissociation. (C) Cell extracts were treated with EDTA to induce ribosome dissociation. Note that *fbp1-as* was detectable in fraction III of CHX-treated but not in that of EDTA-treated cell lysates.

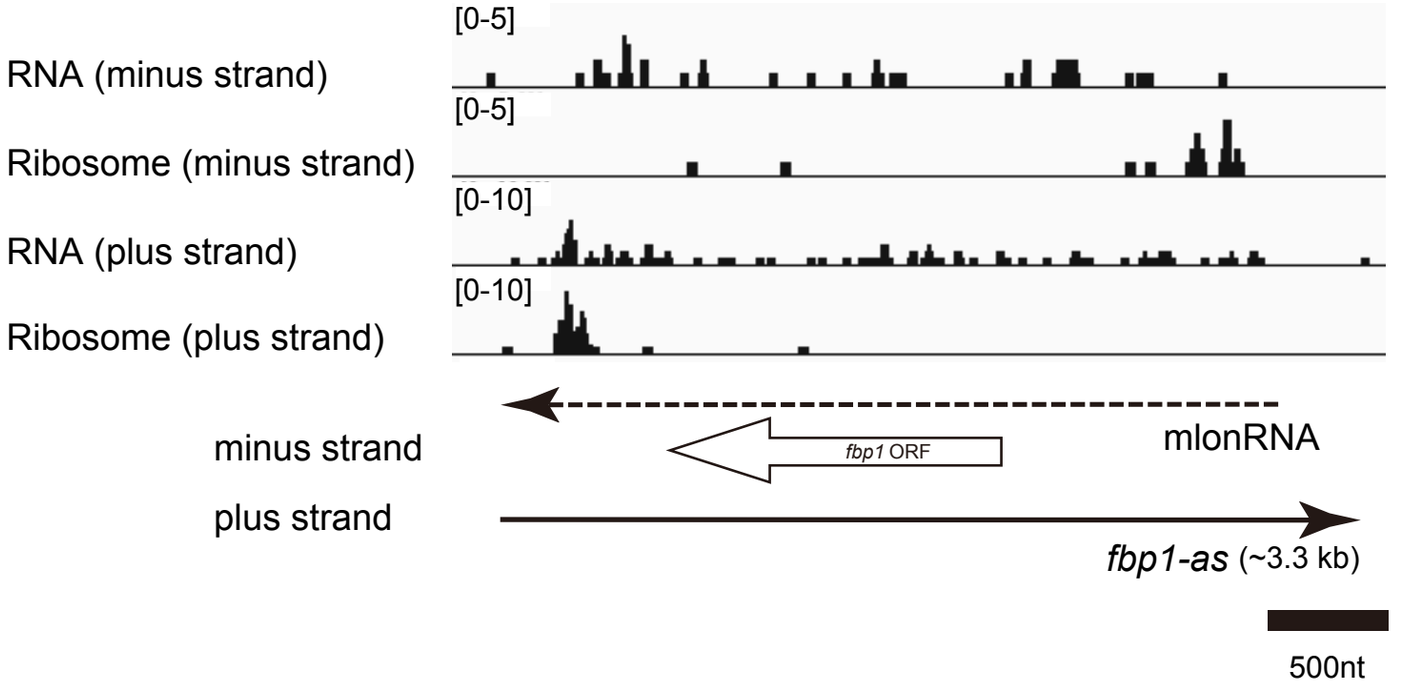

Fig. 17 *fbp1-as* is associated with ribosomes.

Ribosome profiling data at the *fbp1* locus. The data was taken from Subtelny *et al.* 2014. RNA (minus, or plus strand): strand-specific mapping of RNA-seq reads. Ribosome (minus, or plus strand): strand-specific mapping of ribosome profiling (ribo-seq) reads. The range of mapped read counts is indicated in parentheses on the Y-axis. Horizontal broken, open, and solid arrows in the lower part indicate the *fbp1* mlonRNA, mRNA, and *fbp1-as* transcripts, respectively. The scale bar represents 500 nt.

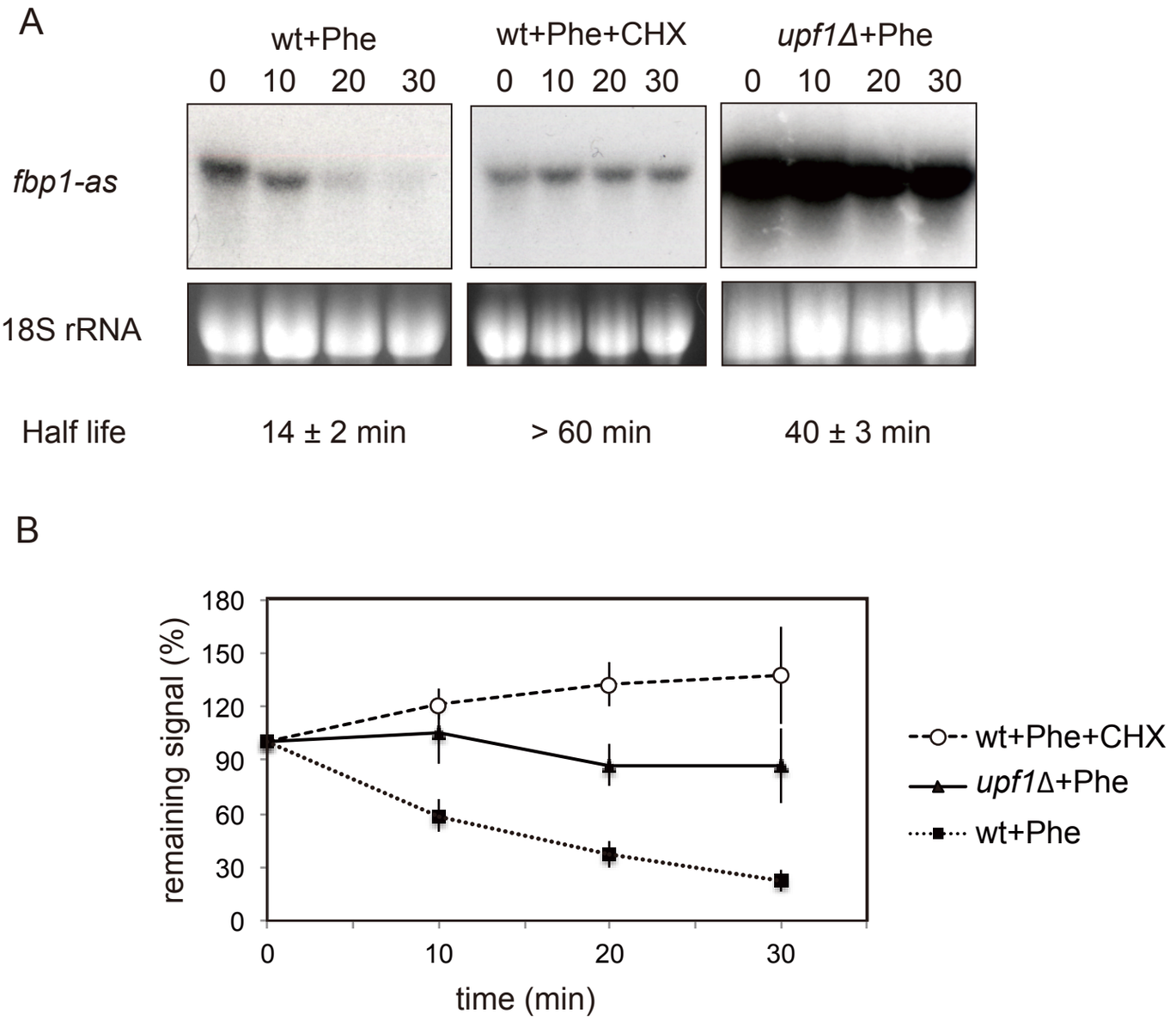

Fig. 18 The degradation of *fbp1-as* is translation-dependent.

A. Top panels: Northern blots using the same strand-specific probe as in Fig. 8. *fbp1-as* half-life measurements in wild type cells treated with 1,10-Phenanthroline (left, wt+Phe), wild type cells treated with Phe and cycloheximide (CHX) (middle, wt+Phe+CHX), *upf1*Δ treated with Phe (right, *upf1*Δ+Phe). Bottom panels: ethidium bromide-stained loading controls showing 18S rRNA.

B. Quantification of the Northern blot signals in (A), showing the remaining signal relative to the signal before drug addition (0 min). Error bars represent the standard deviations of three biological replicates. Solid, dotted, dashed lines represent *upf1*Δ +Phe, wild type +Phe, and wild type +Phe+CHX, respectively.

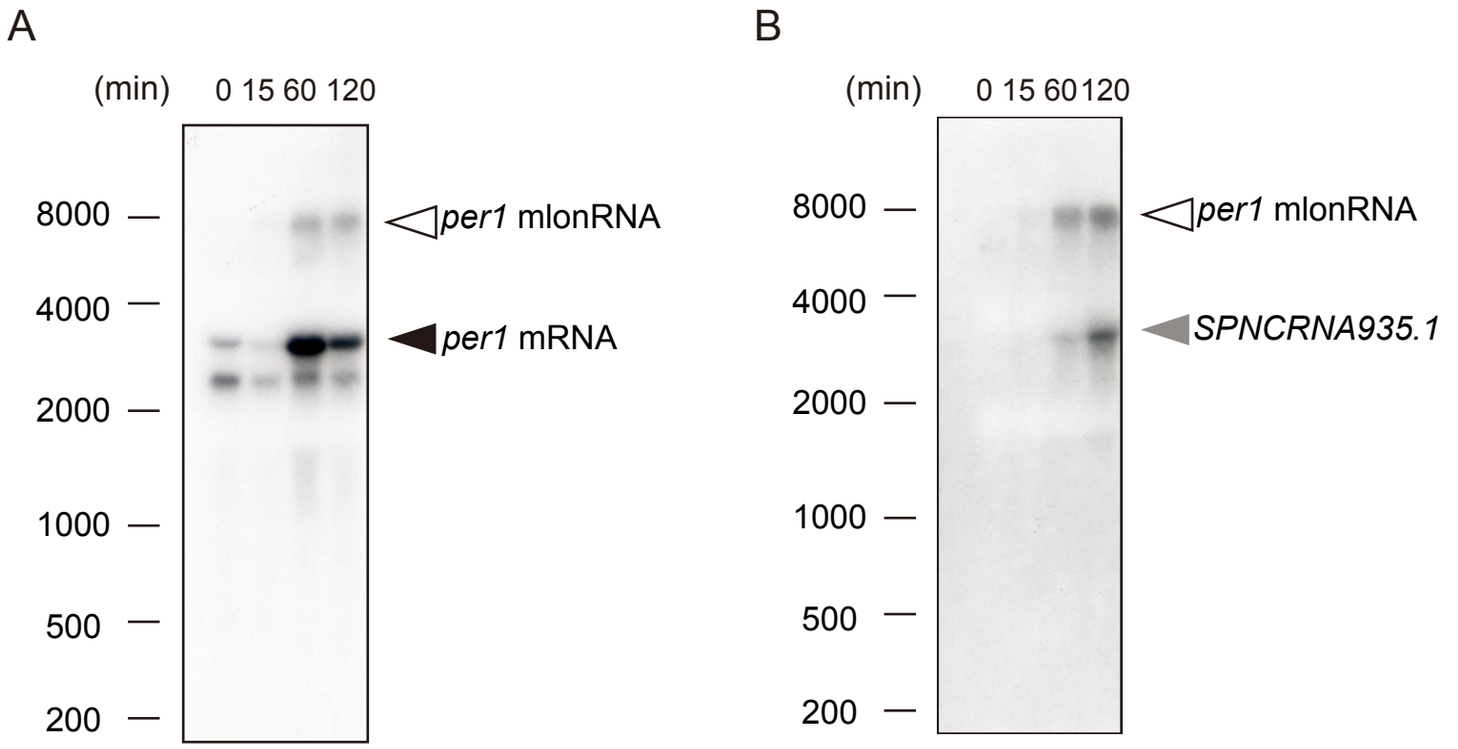

Fig. 19 Detection of *per1* mlonRNA transcripts.

A-B. DNA probe for *per1* mRNA (A) and strand-specific RNA probe for *per1* mlonRNA (C) revealed longer continuous transcripts overlapping both *SPNCRNA935.1* and the *per1* locus (upper open arrow). Wild type cells were shifted from glucose rich medium to glucose poor medium. Time point 0 min corresponds to glucose rich condition; 15, 60, and 120 min correspond to sampling times after the medium shift. The sizes of transcripts (bases) checked by RNA molecular weight ladder are shown on the left part of the blots.

(A) The upper or lower arrow indicates *per1* mlonRNA or mRNA, respectively.

(B) The upper or lower arrow indicates *per1* mlonRNA or *SPNCRNA935.1*, respectively.

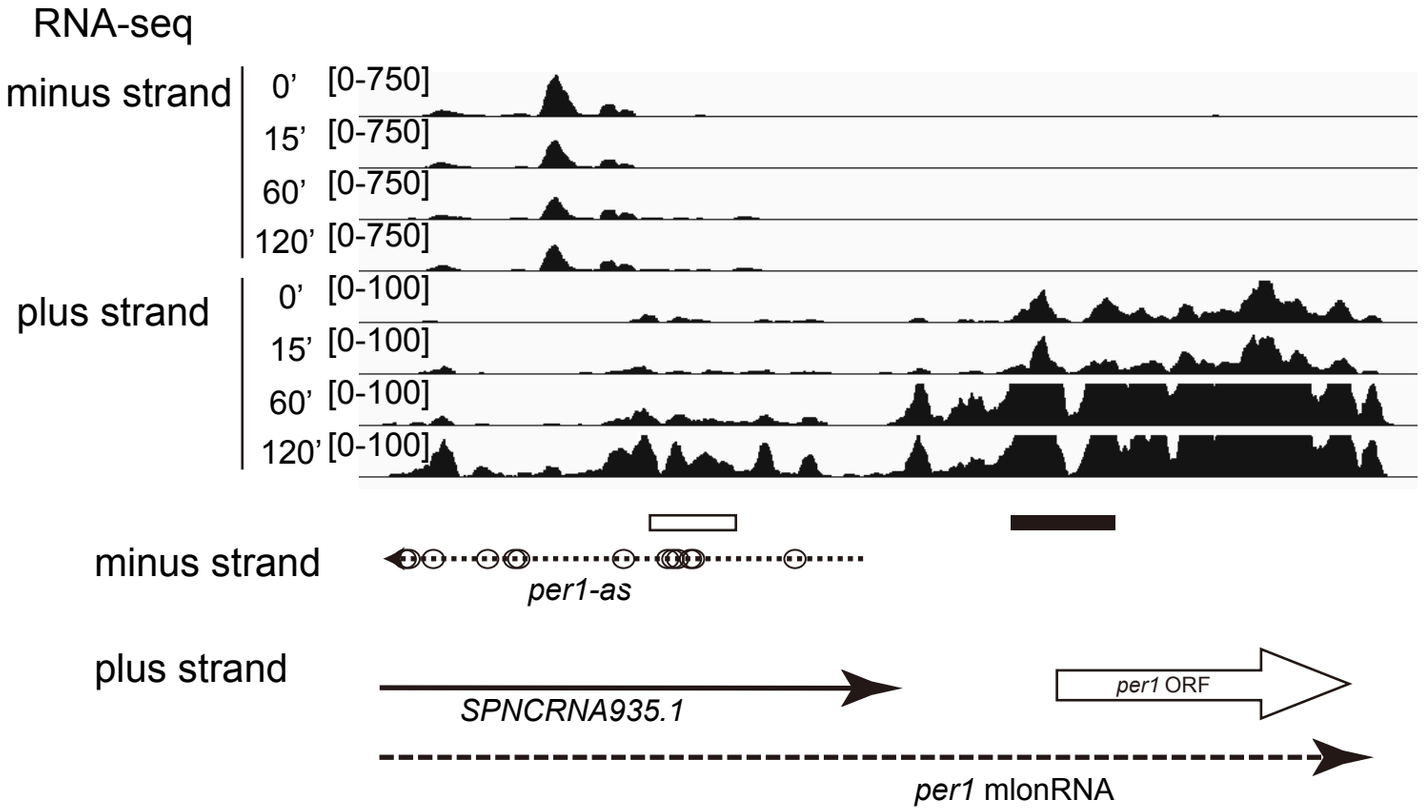

Fig. 20 Detection of *per1* mlonRNA transcripts.

RNA-seq data (Oda *et al*. 2015) of several time points during glucose starvation (0, 15, 60, and 120 min) confirm the anti-correlated pattern of sense-antisense RNA transcription. Upper part: RNA-seq data with the range of mapped read counts indicated in parentheses on the Y-axis. Lower part: Broken, open, solid, and dotted arrows represent the *per1* mlonRNA, mRNA, *SPNCRNA935.1,* and *SPNCRNA934.1 (per1-as),* respectively. Open circles represent small ORFs with more than 20 codons, including the termination codon as in Fig. 13. The location of the probes used for *per1* mRNA or *per1* mlonRNA detection in Fig. 17 is shown in a filled box or in an open box, respectively.

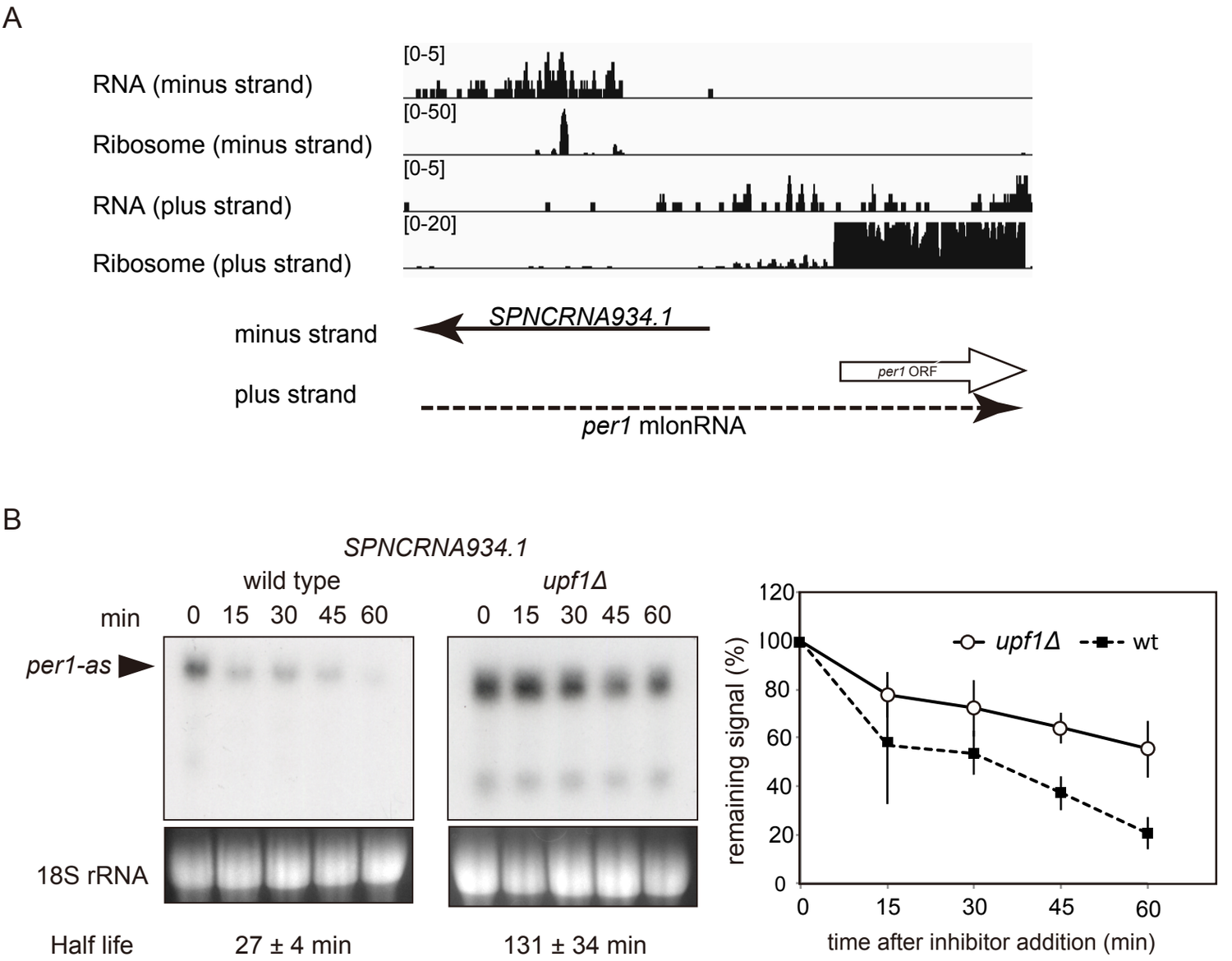

Fig. 21 NMD-dependency of other stress-responsive antisense RNAs.

A. Ribosome profiling data around *per1* region as in Fig. 15. Data obtained from Subtelny *et al.* 2014. RNA (minus, or plus strand): strand-specific mapping of RNA-seq reads. Ribosome (minus, or plus strand): strand-specific mapping of ribosom profiling (ribo-seq) reads. The range of mapped read counts is indicated in parentheses on the Y-axis. The position of the *per1* mlonRNA, mRNA, *SPNCRNA935.1,* and *SPNCRNA934.1 (per1-as)* are indicated as in Fig. 18.

B. Half-life of *SPNCRNA934.1 (per1-as)* in wild type and NMD-defective *upf1*Δ mutant. Remaining signals of *per1-as* in *upf1*Δ (solid line) and wild type (dashed line) are indicated. Quantification data with error bars (standard deviations) were obtained for three biological replicates. The black arrowhead indicates *SPNCRNA934.1 (per1-as)* signal.

SECTION (III) Antisense and sense RNA expression

本章については５年以内に雑誌等で刊行予定のため、非公開。

Discussion

Constitutive degradation of antisense RNAs

To strictly regulate gene expression at the right timing and at the proper level is essential for adaptation to environmental changes. At transcription, localization, and degradation levels, gene expression is regulated. Along with transcriptional factors, some non-coding RNAs play important roles in gene regulation. Antisense RNAs are one of such regulatory non-coding RNAs which are suggested to function at transcription, localization, and degradation levels.

In this paper, I focused on glucose-stress responsive gene loci, from which region both sense and antisense RNAs are expressed in an anti-correlated manner. Antisense RNAs from these regions escape complete nuclear degradation and are exported to the cytoplasm, and there they bound to ribosomes to be degraded by translation-coupled decay (NMD pathway). This degradation is constitutive, as it occurs to the same extent both before and during stress.

These results suggest that the quick switch from antisense to sense RNA expression is achieved by both swift transcriptional suppression and constitutive decay of antisense RNAs. The constitutive RNA decay accelerates the disappearance of antisense RNAs when their transcription is swiftly suppressed upon glucose starvation. This mechanism is opposite to the previously reported fission yeast Mmi1-regulated meiotic gene regulation system, where meiotic inactivation of Mmi1 causes stage-specific expression of some meiosis-specific RNAs by inactivating RNA degradation (Harigaya *et al.* 2006).

However, it should be noted that both systems highlight the importance of RNA degradation in gene expression.

An even more interesting point is that these antisense RNAs from stress-responsive loci including *fbp1-as* extensively associate with ribosomes. In the past few years, what was previously thought as non-coding RNAs turned out to express unannotated peptides, and these peptides are sometimes important for cellular adaptation to environmental changes. For instance, short peptides originating from non-coding RNAs in muscle tissue were shown to regulate the activity of ion channel of the cell surface (Nelson *et al*. 2016). Further analysis would reveal the importance of ribosome association with non-coding RNAs.

Unexpectedly, the steady state level of *fbp1-as* did not change in *exo2Δ*, since Exo2-target RNAs should be accumulated steadily in *exo2Δ*, like observed in other mutants for RNA decay pathways, such as *rrp6Δ* (nuclear exosome cofactor deletion) or *upf1Δ* (NMD-deficient) strain. This paradox may be explained by decrease of *fbp1-as* transcription in *exo2*Δ. Indeed, it was reported that *S. cerevisiae* Exo2 homolog Xrn1 stimulates transcription by directly associating with chromatin (Haimovich *et al*. 2013). Future research is warranted to confirm whether Exo2 is a positive regulator for stress-responsive transcription of antisense noncoding RNA including *fbp1* locus.

References

Arigo, J.T., Eyler, D.E., Carroll, K.L. & Corden, J.L. (2006) Termination of cryptic unstable transcripts is directed by yeast RNA-binding proteins Nrd1 and Nab3. *Mol Cell* **23**, 841-851.

Aspden, J.L., Eyre-Walker, Y.C., Phillips, R.J., Amin, U., Mumtaz, M.A.S., Brocard, M. & Couso, J. P. (2014) Extensive translation of small open reading frames revealed by Poly-Ribo-Seq. *eLife* **3**, e03528.

Bentley, D.L. (2005) Rules of engagement: co-transcriptional recruitment of pre-mRNA processing factors. *Curr. Opin. Cell Biol.* **17**, 251-256.

Berretta, J. & Morillon, A. (2009) Pervasive transcription constitutes a new level of eukaryotic genome regulation. *EMBO reports* **10**, 973-982.

Bitton, D.A., Grallert, A., Scutt, P.J., Yates, T., Li, Y., Bradford, J.R., Hey, Y., Pepper, S.D., Hagan, I.M. & Miller, C.J. (2011) Programmed fluctuations in sense/antisense transcript ratios drive sexual differentiation in *S. pombe*. *Mol. Sys. Biol.* **7**, 559

Brimacombe, R. & Stiege, W. (1985) Structure and function of ribosomal RNA.

Taft, R.J., Pheasant, M. & Mattick, J.S. (2007) The relationship between non-protein-coding DNA and eukaryotic complexity. *BioEssays* **29**, 288-299.

Brogna, S. & Wen, J. (2009) Nonsense-mediated mRNA decay (NMD) mechanisms. *Nat. Struct. Mol. Biol.* **16**, 107-113.

Bühler, M., Spies, N., Bartel, D.P. & Moazed, D. (2008) TRAMP-mediated RNA

surveillance prevents spurious entry of RNAs into the *Schizosaccharomyces pombe* siRNA pathway. *Nat. Struct. Mol. Biol.* **15**, 1015-1023.

Carrieri, C., Cimatti, L., Biagioli, M., Beugnet, A., Zucchelli, S., Fedele, S., Pesce, E., Ferrer, I., Collavin, L., Santoro, C., Forrest, A.R.R., Carninci, P., Biffo, S., Stupka, E. & Gustincich, S. (2012) Long non-coding antisense RNA controls Uchl1 translation through an embedded *SINEB2* repeat. *Nature* **491**, 454-457.

Duncan, C.D.S. & Mata, J. (2014) The translational landscape of fission-yeast meiosis and sporulation. *Nat. Struct. Mol. Biol.* **21**, 641-647.

Fox, M.J., Gao, H., Smith-Kinnaman, W.R., Liu, Y. & Mosley, A.L. (2015) The exosome component Rrp6 is required for RNA polymerase II termination at specific targets of the Nrd1-Nab3 Pathway. *PLOS Genet* **11**, e1004999.

Gaba, A., Jacobson, A. & Sachs, M.S. (2005) Ribosome occupancy of the yeast CPA1 upstream open reading frame termination codon modulates nonsense-mediated mRNA decay. *Mol. cell* **20**, 449-460.

Galipon, J., Miki, A., Oda, A., Inada, T. & Ohta, K. (2013) Stress-induced lncRNAs evade nuclear degradation and enter the translational machinery. *Genes Cells* **18**, 353-368.

Gall, J.G. (1981) Chromosome structure and the C-value paradox. *J Cell Biol* **91**, 3s.

Guttman, M., Russell, P., Ingolia, N.T., Weissman, J.S. & Lander, E.S. (2013) Ribosome profiling provides evidence that large non-coding RNAs do not encode proteins. *Cell* **154**, 240-251.

Hai, T.W., Liu, F., Allegretto, E.A., Karin, M. & Green, M.R. (1988) A family of immunologically related transcription factors that includes multiple forms of ATF and AP-1. *Genes & Development* **2**, 1216-1226.

Haimovich, G., Medina, D.A., Causse, S.Z., Garber, M., Millan-Zambrano, G., Barkai, O., Chavez, S., Perez-Ortin, J.E., Darzacq, X. & Choder, M. (2013) Gene expression is circular: factors for mRNA degradation also foster mRNA synthesis. *Cell* **153**, 1000-1011.

Harigaya, Y., Tanaka, H., Yamanaka, S., Tanaka, K., Watanabe, Y., Tsutsumi, C., Chikashige, Y., Hiraoka, Y., Yamashita, A., and Yamamoto, M. (2006). Selective elimination of messenger RNA prevents an incidence of untimely meiosis. *Nature* **442**, 45-50.

Hasan, A., Cotobal, C., Duncan, C.D.S. & Mata, J. (2014) Systematic analysis of the role of RNA-binding proteins in the regulation of RNA stability. *PLoS Genet.* **10**, e1004684.

Heinrich, S., Geissen, E.M., Kamenz, J., Trautmann, S., Widmer, C., Drewe, P., Knop, M., Radde, N., Hasenauer, J. & Hauf, S. (2013) Determinants of robustness in spindle assembly checkpoint signalling. *Nat. Cell Biol.* **15**, 1328-1339.

Heiman, M., Schaefer, A., Gong, S., Peterson, J.D., Day, M., Ramsey, K.E., Suárez-Fariñas, M., Schwarz, C., Stephan, D.A., Surmeier, D.J., Greengard, P. & Heintz, N. (2008) A translational profiling approach for the molecular characterization of CNS cell types. *Cell* **135**, 738-748.

Higuchi, T., Watanabe, Y. & Yamamoto, M. (2002) Protein kinase A regulates sexual development and gluconeogenesis through phosphorylation of the Zn finger transcriptional activator Rst2p in fission yeast. *Mol cell boil* **22**, 1-11.

Hirota, K., Hoffman, C.S., Shibata, T. & Ohta, K. (2003) Fission yeast Tup1-Like repressors repress chromatin remodeling at the *fbp1*$^{+}$ promoter and the ade6-M26 recombination hotspot. *Genetics* **165**, 505-515.

Hirota, K., Miyoshi, T., Kugou, K., Hoffman, C.S., Shibata, T. & Ohta, K. (2008) Stepwise chromatin remodelling by a cascade of transcription initiation of non-coding RNAs. *Nature* **456**, 130-134.

Hobson, David J., Wei, W., Steinmetz, Lars M. & Svejstrup, Jesper Q. (2012) RNA polymerase II collision interrupts convergent transcription. *Mol. Cell* **48**, 365-374.

Holley, R.W., Apgar, J., Everett, G.A., Madison, J.T., Marquisee, M., Merrill, S.H., Penswick, J.R. & Zamir, A. (1965) Structure of a ribonucleic acid. *Science* **147**, 1462.

Hongay, C.F., Grisafi, P.L., Galitski, T. & Fink, G.R. (2006) Antisense Transcription controls cell fate in Saccharomyces cerevisiae. *Cell* **127**, 735-745.

Houseley, J., LaCava, J. & Tollervey, D. (2006) RNA-quality control by the exosome. *Nat. Rev. Mol. Cell Biol.* **7**, 529-539.

Huber, F., Bunina, D., Gupta, I., Khmelinskii, A., Meurer, M., Theer, P., Steinmetz, Lars M. & Knop, M. (2016) Protein abundance control by non-coding

antisense transcription. *Cell reports* **15**, 2625-2636.

Kebaara, B.W. & Atkin, A.L. (2009) Long 3'-UTRs target wild-type mRNAs for nonsense-mediated mRNA decay in *Saccharomyces cerevisiae*. *Nucleic Acids Res.* **37**, 2771-2778.

Kondo, T., Plaza, S., Zanet, J., Benrabah, E., Valenti, P., Hashimoto, Y., Kobayashi, S., Payre, F. & Kageyama, Y. (2010) Small peptides switch the transcriptional activity of Shavenbaby during Drosophila embryogenesis. *Science* **329**, 336.

Kretz, M., Siprashvili, Z., Chu, C. *et al.* (2013) Control of somatic tissue differentiation by the long non-coding RNA TINCR. *Nature* **493**, 231-235.

Krinke, L. & Wulff, D.L. (1987) OOP RNA, produced from multicopy plasmids, inhibits lambda cII gene expression through an RNase III-dependent mechanism. *Genes. Dev.* **1**, 1005-1013.

Krogan, N.J., Kim, M., Tong, A., Golshani, A., Cagney, G., Canadien, V., Richards, D.P., Beattie, B.K., Emili, A., Boone, C., Shilatifard, A., Buratowski, S. & Greenblatt, J. (2003) Methylation of histone H3 by Set2 in *Saccharomyces cerevisiae* is linked to transcriptional tlongation by RNA Polymerase II. *Mol Cell Biol* **23**, 4207-4218.

Kung, J.T.Y., Colognori, D. & Lee, J.T. (2013) Long noncoding RNAs: Past, Present, and Future. *Genetics* **193**, 651.

Lee, J.T. & Lu, N. (1999) Targeted mutagenesis of Tsix leads to nonrandom X inactivation. *Cell* **99**, 47-57.

Lejeune, F., Li, X. & Maquat, L.E. (2003) Nonsense-mediated mRNA decay in mammalian cells involves decapping, deadenylating, and exonucleolytic activities. *Mol. cell* **12**, 675-687.

Leong, H.S., Dawson, K., Wirth, C., Li, Y., Connolly, Y., Smith, D.L., Wilkinson, C.R.M. & Miller, C.J. (2014) A global non-coding RNA system modulates fission yeast protein levels in response to stress. *Nat. Commun.* **5,** 3947

Medenbach, J., Seiler, M. & Hentze, Matthias W. (2011) Translational control via protein-regulated upstream open reading frames. *Cell* **145**, 902-913.

Millar, J.B., Buck, V. & Wilkinson, M.G. (1995) Pyp1 and Pyp2 PTPases dephosphorylate an osmosensing MAP kinase controlling cell size at division in fission yeast. *Genes. Dev.* **9**, 2117-2130.

Mueller, F., Senecal, A., Tantale, K., Marie-Nelly, H., Ly, N., Collin, O., Basyuk, E., Bertrand, E., Darzacq, X. & Zimmer, C. (2013) FISH-quant: automatic counting of transcripts in 3D FISH images. *Nat. Meth*. **10**, 277-278.

Muhlrad, D. & Parker, R. (1994) Premature translational termination triggers mRNA decapping. *Nature* **370**, 578-581.

Muhlrad, D. & Parker, R. (1999) Aberrant mRNAs with extended 3' UTRs are substrates for rapid degradation by mRNA surveillance. *RNA* **5**, 1299-1307.

Murray, S.C., Haenni, S., Howe, F.S., Fischl, H., Chocian, K., Nair, A. & Mellor, J. (2015) Sense and antisense transcription are associated with distinct chromatin architectures across genes. *Nucleic Acids Res*. **43**, 7823-7837.

Neely, L.A. & Hoffman, C.S. (2000) Protein Kinase A and mitogen-activated

protein kinase pathways antagonistically regulate fission yeast *fbp1* transcription by employing different modes of action at two upstream activation sites. *Mol cell biol* **20**, 6426-6434.

Nelson, B.R., Makarewich, C.A., Anderson, D.M., Winders, B.R., Troupes, C.D., Wu, F., Reese, A.L., McAnally, J.R., Chen, X., Kavalali, E.T., Cannon, S.C., Houser, S.R., Bassel-Duby, R. & Olson, E.N. (2016) A peptide encoded by a transcript annotated as long noncoding RNA enhances SERCA activity in muscle. *Science* **351**, 271.

Ng, H.H., Robert, F., Young, R.A. & Struhl, K. (2003) Targeted recruitment of Set1 histone methylase by elongating pol II provides a localized mark and memory of recent transcriptional activity. *Mol Cell* **11**, 709-719.

Ni, T., Tu, K., Wang, Z., Song, S., Wu, H., Xie, B., Scott, K.C., Grewal, S.I., Gao, Y. & Zhu, J. (2010) The prevalence and regulation of antisense transcripts in *Schizosaccharomyces pombe*. *PLoS One* **5**, e15271.

Oda, A., Takemata, N., Hirata, Y., Miyoshi, T., Suzuki, Y., Sugano, S. & Ohta, K. (2015) Dynamic transition of transcription and chromatin landscape during fission yeast adaptation to glucose starvation. *Genes Cells* **20**, 392-407.

Parker, R. (2012) RNA degradation in *Saccharomyces cerevisae*. *Genetics* **191**, 671-702.

Preker, P., Nielsen, J., Kammler, S., Lykke-Andersen, S., Christensen, M.S., Mapendano, C.K., Schierup, M.H. & Jensen, T.H. (2008) RNA exosome

depletion reveals transcription upstream of active human promoters. *Science* **322**, 1851-1854.

Raj, A., van den Bogaard, P., Rifkin, S.A., van Oudenaarden, A. & Tyagi, S. (2008) Imaging individual mRNA molecules using multiple singly labeled probes. *Nature methods* **5**, 877-879.

Rhind, N., Chen, Z., Yassour, M. *et al.* (2011) Comparative functional genomics of the fission yeasts. *Science* **332**, 930-936.

Rinn, J.L., Kertesz, M., Wang, J.K., Squazzo, S.L., Xu, X., Brugmann, S.A., Goodnough, L.H., Helms, J.A., Farnham, P.J., Segal, E. & Chang, H.Y. (2007) Functional demarcation of active and silent chromatin domains in human *HOX* loci by noncoding RNAs. *Cell* **129**, 1311-1323.

Rodríguez-Gabriel, M.A., Watt, S., Bähler, J. & Russell, P. (2006) Upf1, an RNA helicase required for nonsense-mediated mRNA decay, modulates the transcriptional response to oxidative stress in fission yeast. *Mol. Cell. Biol.* **26**, 6347–6356.

Roesler, W., Vandenbark, G. & Hanson, R.W. (1988) Cyclic AMP and the induction of eukaryotic gene transcription. *J Biol Chem* **263**, 9063-9066.

Samejima, I., Mackie, S. & Fantes, P.A. (1997) Multiple modes of activation of the stress-responsive MAP kinase pathway in fission yeast. *EMBO J* **16**, 6162.

Samejima, I., Mackie, S., Warbrick, E., Weisman, R. & Fantes, P.A. (1998) The fission yeast mitotic regulator *win1*$^{+}$ encodes an MAP Kinase Kinase Kinase that

phosphorylates and activates Wis1 MAP Kinase Kinase in response to high osmolarity. *Mol Biol Cell* **9**, 2325-2335.

Schoenberg, D.R. & Maquat, L.E. (2012) Regulation of cytoplasmic mRNA decay. *Nat. Rev. Genet.* **13**, 246-259.

Schulz, D., Schwalb, B., Kiesel, A., Baejen, C., Torkler, P., Gagneur, J., Soeding, J. & Cramer, P. (2013) Transcriptome surveillance by selective termination of noncoding RNA synthesis. *Cell* **155**, 1075-1087.

Shiozaki, K. & Russell, P. (1995) Cell-cycle control linked to extracellular environment by MAP kinase pathway in fission yeast. *Nature* **378**, 739-743.

Shiozaki, K. & Russell, P. (1996) Conjugation, meiosis, and the osmotic stress response are regulated by Spc1 kinase through Atf1 transcription factor in fission yeast. *Genes & Development* **10**, 2276-2288.

Smith, J.E., Alvarez-Dominguez, J.R., Kline, N., Huynh, N.J., Geisler, S., Hu, W., Coller, J. & Baker, K.E. (2014) Translation of small open reading frames within unannotated RNA transcripts in Saccharomyces cerevisiae. *Cell Reports* **7**, 1858-1866.

Smith, J.E. & Baker, K.E. (2015) Nonsense-mediated RNA decay--a switch and dial for regulating gene expression. *Bioessays* **37**, 612-623.

Su, W.Y., Li, J.T., Cui, Y., Hong, J., Du, W., Wang, Y.C., Lin, Y.W., Xiong, H., Wang, J.L., Kong, X., Gao, Q.Y., Wei, L.P. & Fang, J.Y. (2012) Bidirectional regulation between WDR83 and its natural antisense transcript DHPS in gastric cancer. *Cell Res* **22**, 1374-1389.

Subtelny, A.O., Eichhorn, S.W., Chen, G.R., Sive, H. & Bartel, D.P. (2014) Poly(A)-tail profiling reveals an embryonic switch in translational control. *Nature* 508, 66-71.

Swiezewski, S., Liu, F., Magusin, A. & Dean, C. (2009) Cold-induced silencing by long antisense transcripts of an Arabidopsis Polycomb target. *Nature* **462**, 799-802.

Takeda, T., Toda, T., Kominami, K. I., Kohnosu, A., Yanagida, M. & Jones, N. (1995) Schizosaccharomyces pombe *atf1*$^{+}$ encodes a transcription factor required for sexual development and entry into stationary phase. *EMBO J.* **14**, 6193.

Takemata, N., Oda, A., Yamada, T., Galipon, J., Miyoshi, T., Suzuki, Y., Sugano, S., Hoffman, C.S., Hirota, K. & Ohta, K. (2016) Local potentiation of stress-responsive genes by upstream noncoding transcription. *Nucleic Acids Res*. **44** (11): 5174-5189.

Taniue, K., Kurimoto, A., Sugimasa, H., Nasu, E., Takeda, Y., Iwasaki, K., Nagashima, T., Okada-Hatakeyama, M., Oyama, M., Kozuka-Hata, H., Hiyoshi, M., Kitayama, J., Negishi, L., Kawasaki, Y. & Akiyama, T. (2016) Long noncoding RNA UPAT promotes colon tumorigenesis by inhibiting degradation of *UHRF1*. *Proc. Natl. Acad. Sci. USA* **113**, 1273-1278.

Tomizawa, J., Itoh, T., Selzer, G. & Som, T. (1981) Inhibition of ColE1 RNA primer formation by a plasmid-specified small RNA. *Proc. Natl. Acad. Sci. USA* **78**, 1421-1425.

Tsai, M.C., Manor, O., Wan, Y., Mosammaparast, N., Wang, J.K., Lan, F., Shi, Y., Segal, E. & Chang, H.Y. (2010) Long noncoding RNA as modular scaffold of histone modification complexes. *Science* **329**, 689-693.

Tufarelli, C., Stanley, J.A.S., Garrick, D., Sharpe, J.A., Ayyub, H., Wood, W.G. & Higgs, D.R. (2003) Transcription of antisense RNA leading to gene silencing and methylation as a novel cause of human genetic disease. *Nat Genet* **34**, 157-165.

Uhler, J.P., Hertel, C. & Svejstrup, J.Q. (2007) A role for noncoding transcription in activation of the yeast PHO5 gene. *Proc. Natl. Acad. Sci. USA* **104**, 8011-8016.

van Dijk, E.L., Chen, C.L., d'Aubenton-Carafa, Y., Gourvennec, S., Kwapisz, M., Roche, V., Bertrand, C., Silvain, M., Legoix-Ne, P., Loeillet, S., Nicolas, A., Thermes, C. & Morillon, A. (2011) XUTs are a class of Xrn1-sensitive antisense regulatory non-coding RNA in yeast. *Nature* **475**, 114-117.

Vasiljeva, L. & Buratowski, S. (2006) Nrd1 interacts with the nuclear exosome for 3′ processing of RNA Polymerase II transcripts. *Mol Cell* **21**, 239-248

Verdel, A., Jia, S., Gerber, S., Sugiyama, T., Gygi, S., Grewal, S.I.S. & Moazed, D. (2004) RNAi-mediated targeting of heterochromatin by the RITS complex. *Science* **303**, 672.

Warbrick, E. & Fantes, P.A. (1991) The wis1 protein kinase is a dosage-dependent regulator of mitosis in Schizosaccharomyces pombe. *EMBO J.* **10**, 4291-4299.

Watanabe, Y. & Yamamoto, M. (1996) Schizosaccharomyces pombe pcr1+ encodes a CREB/ATF protein involved in regulation of gene expression for sexual development. *Mol cell biol* **16**, 704-711.

Welton, R.M. & Hoffman, C.S. (2000) Glucose monitoring in fission yeast via the Gpa2 Galpha, the git5 Gbeta and the git3 putative glucose receptor. *Genetics* **156**, 513-521.

Wery, M., Descrimes, M., Vogt, N., Dallongeville, A.S., Gautheret, D. & Morillon, A. (2016) Nonsense-mediated decay restricts lncRNA levels in yeast unless blocked by double-stranded RNA structure. *Mol. Cell* **61**, 379-392.

Wyers, F., Rougemaille, M., Badis, G., Rousselle, J.C., Dufour, M. E., Boulay, J., Régnault, B., Devaux, F., Namane, A., Séraphin, B., Libri, D. & Jacquier, A. (2005) Cryptic pol II transcripts are degraded by a nuclear quality control pathway involving a new poly(A) polymerase. *Cell* **121**, 725-737.

Xu, Z., Wei, W., Gagneur, J., Perocchi, F., Clauder-Munster, S., Camblong, J., Guffanti, E., Stutz, F., Huber, W. & Steinmetz, L.M. (2009) Bidirectional promoters generate pervasive transcription in yeast. *Nature* **457**, 1033-1037.

Yap, K.L., Li, S., Muñoz-Cabello, A.M., Raguz, S., Zeng, L., Mujtaba, S., Gil, J., Walsh, M.J. & Zhou, M.M. (2010) Molecular interplay of the noncoding RNA ANRIL and methylated histone H3 lysine 27 by polycomb CBX7 in transcriptional ailencing of INK4a. *Mol cell* **38**, 662-674.

Yoon, J.H., Abdelmohsen, K., Srikantan, S., Yang, X., Martindale, J.L., De, S., Huarte, M., Zhan, M., Becker, K.G. & Gorospe, M. (2012) LincRNA-p21

suppresses target mRNA translation. *Mol. Cell* **47**, 648-655.

Zhang, K., Mosch, K., Fischle, W. & Grewal, S.I.S. (2008) Roles of the Clr4 methyltransferase complex in nucleation, spreading and maintenance of heterochromatin. *Nat Struct Mol Biol* **15**, 381-388.

Zhang, Y., Liu, X.S., Liu, Q.R. & Wei, L. (2006) Genome-wide in silico identification and analysis of cis natural antisense transcripts (cis-NATs) in ten species. *Nucleic Acids Res.* **34**, 3465-3475.

Acknowledgements

I would like to express my deep gratitude to Professor Kunihiro Ohta, who guided and helped me for five years with a positive atmosphere. My appreciation also extends to Dr. Josephine Galipon, who mentored me with her enthusiasm for biology. I would also like to express my sincere appreciation to Dr. Satoshi Sawai and Dr. Toshifumi Inada for collaborating with me.

I am grateful to Dr. Masayuki Yamamoto, Dr. Jurg Bähler, Dr. Takatomi Yamada, and Dr. Arisa Oda for providing strains, as well as Dr. Kosuke Oana, Dr. Kazuki Motomura, and Dr. Yukihide Tomari for sharing the polysome fractionation protocol. The single molecule FISH procedure was a courtesy of Dr. Stephanie Heinrich, Dr. Hauf Silke, Dr. Sandra Rima Imrazene and Dr. Daniel Zenklusen.

I would like to thank Dr. Ryosuke Sato, Dr. Reiko Sugiura, Dr. Shao Win Wang, and Dr. François Bachand for sharing strains, though the experiments using those strains were not included in this thesis. I also thank Dr. Arisa Oda for advice on computational analyses and all laboratory members for helpful discussions and technical support. I am also grateful to my friends, who encourage my research at meetings or other occasions. Finally, I am deeply indebted to my family for supporting my five years of graduate research.